TRABAJO DE FIN DE MASTER

Protección sísmica de muros de mampostería para estructuras ubicadas en zonas de alta peligrosidad sísmica en España, aplicable a un edificio en el sur de la provincia de Alicante.

Presentado por

Hurtado Orts, Inés

Para la obtención del

Máster en Ingeniería de Caminos, Canales y Puertos

Curso: 2018/2019

Fecha: Julio 2019

Tutor: Luis Pallarés Rubio

Cotutor: Enrico Tubaldi

CONTENTS

FIGURES

TABLES

1. ABSTRACT

The main purpose of this project consists of developing numerical models of masonry infill walls by using the software Abaqus. These models will be compared to experimental models which were carried out in the University of Padova in Italy as part of the INSYSME project (INSYSME, 2013).

Two different approaches are studied: macroscale and mesoscale models. Inside each of these approaches, two different walls are developed. Firstly, a masonry infill wall designed with mortar joints. Secondly, the same wall but with the addition of rubber joints in order to evaluate the reduction of the infill damage during a seismic event thanks to the inclusion of these special joints.

This report will focus on loads acting perpendicularly on walls, which are known as out-of-plane loads. For the macroscale models, the seismic event is represented by out-of-plane loads acting on the walls. However, for the mesoscale models, the out-of-plane load is applied once the wall has been damaged by a load acting on its own plane, called in-plane load. In-plane and out-of-plane loads represent a seismic event for the mesoscale models and the results obtained can be compared to the experimental ones, where both in-plane and out-of-plane loads were applied.

The efficiency of rubber joints will be analysed after developing the models. Macroscale models will allow to assess if the addition of rubber joints does imply a better behaviour of the wall against out-of-plane loads. Mesoscale models will also be carried out in order to evaluate if the results can be compared to the experimental ones, studying how accurately they replicate the behaviour of walls against seismic loading. In case of demonstrating beneficial characteristics, the addition of rubber joints in masonry infill walls can be an innovative system that increases the safety of different structures located in areas of high seismic hazard such as the province of Alicante in Spain.

2. INTRODUCTION

Masonry infills are widely used in reinforced concrete framed buildings. Masonry has an excellent performance as an insulation material, protecting the inside of buildings from temperature, noise and fire among others. Masonry enclosures have demonstrated to have a good durability and they are commonly used for façades in buildings (INSYSME, n.d.).

According to Pujol et al., (2008), several researches have shown that reinforced concrete frame walls with masonry infill have a greater strength and stiffness compared to bare reinforced concrete frames. However, if masonry infill enclosures are not properly designed, they can become a significant hazard under seismic action. It is essential to study the structural behaviour of the enclosure, to make sure it can accommodate and withstand seismic loads during an earthquake (INSYSME, n.d.).

The University of Padova has been developing several innovative solutions to be introduced in the masonry infill walls so that the damage they suffer during a seismic event can be reduced. A proposed solution consisted of developing experimental models of several masonry infill walls with and without rubber joints in order to study if the addition of these elements has a beneficial impact on masonry enclosures.

3. EXPERIMENTAL MODELS

In 2013, the University of Padova started developing experimental tests in which different walls were subjected to quasi-static loads. These tests were carried out in masonry infill walls as well as in bare wall frames (INSYSME, 2013). The purpose of the project consisted of studying the response of walls to seismic loading. In order to do so, the walls had to withstand loads acting on the same plane, which are known as in-plane loads, and loads acting perpendicularly to them, called out-of-plane loads. Two main walls were studied: one masonry infill wall with mortar joints and another masonry infill wall that included rubber joints.

Figure 1. Experimental tests carried out in the University of Padova (INSYSME, 2013: p.5).

3.1. Properties and dimensions of walls

3.1.1. Wall with mortar joints

This wall is composed of three main elements: a reinforced concrete frame, masonry infill and mortar joints. It is a traditional wall in which the surfaces of the bricks are connected by mortar, as well as the lateral surfaces between bricks and the reinforced concrete frame.

3.1.1.1. Reinforced concrete frame

The frame is the main structure of the wall, which is filled with the different rows of bricks. It has a span of 4150 mm clear and a height of 2750 mm (Verlato et al., 2016). This reinforced concrete frame was considered to be part of a reference 3 storey concrete frame building, which was designed according to the *D.M. 14 gennaio 2008* (Norme Techniche per le Costruzioni, 2008) in high ductility class.

It is based on two beams and two columns. Both columns have the same dimensions. However, the upper and lower beams are not identical, showing different lengths as well as different cross sections.

Columns have a cross section of 30cm x 30cm. Inside each column, there is longitudinal and transverse reinforcement. The longitudinal reinforcement is based on 8 bars of 22 mm of diameter (8Φ22) equally distributed in the cross section (INSYSME, 2013).

The transverse reinforcement is not constant all along the columns. As they approach the beams, the stirrups are separated a smaller distance as the contact area between columns and beams requires of more reinforcement because of being a zone of concentration of tensions. Not only is the distance between stirrups reduced in these areas but also the diameter of the bars increases. The transverse reinforcement is based on:

- Stirrups with a diameter of 10 mm located every 100 mm (Φ10/100 mm) in the contact areas between columns and beams.
- Stirrups with a diameter of 8 mm distanced 150 mm (Φ8/150 mm).
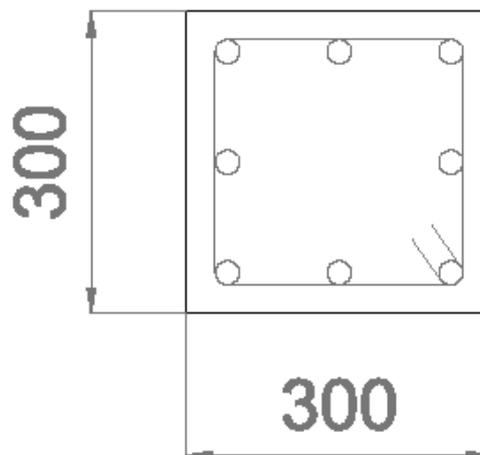
Figure 2. Cross section of columns. Dimensions in mm.

The top beam has a cross section of 50cm x 25cm. As it happens with the columns, there is longitudinal and transverse reinforcement inside this beam. The longitudinal reinforcement consists of 8 bars of 16 mm of diameter (8Φ16) and it is constant all along the beam (INSYSME, 2013).

The transverse reinforcement does change inside the top beam. The distance between stirrups is again smaller as the beam approaches the columns. This transverse reinforcement is designed with:

- Stirrups with a diameter of 8 mm every 80 mm (Φ8/80 mm) in the contact areas between columns and beam.
- Stirrups with a diameter of 8 mm distanced 150 mm (Φ8/150 mm).
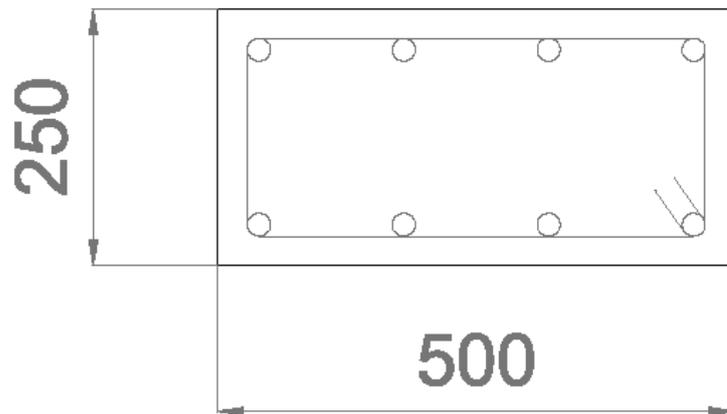
Figure 3. Cross section of top beam. Dimensions in mm.

The concrete used in order to create the frame is C30/35. The steel of the reinforcement bars and stirrups is B450C (INSYSME, 2013).

3.1.1.2. Mortar

The mortar used in the experimental models is a masonry mortar of class M 10 (Verlato et al., 2016). The compressive strength of this class of mortar is 10 N/mm^2 and it is based on a mixture of one or more inorganic binders, water, aggregates and sometimes it can also include additions and/ or admixtures. The proportion of these constituents is declared by the manufacturer (British Standards Institution, 2016).

This mortar is used for bed joints between bricks and it is also placed between the bricks and the reinforced concrete frame.

3.1.1.3. Masonry infill

The masonry infill is based on single-leaf thick clay masonry bricks which are vertically perforated (Verlato et al., 2016). These bricks have a height of 265 mm, a length of 415 mm and a thickness of 300 mm, which is the same as the depth of the columns. The Young's Modulus of the masonry (Em) is 1500 MPa and the Yield Stress (fm) is -1.5 MPa (INSYSME, 2013).

There is only one brick unit used in the experimental models. This brick unit is adapted to the dimensions of the reinforced concrete frame so that it perfectly fits the frame. The total number of brick rows introduced in the experimental mortar model are 13.5.
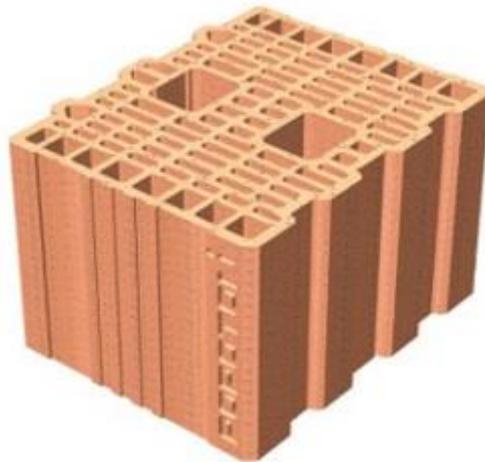
Figure 4. Single-leaf clay brick used in the experimental models (INSYSME, 2013: p.6).

3.1.2. Wall with rubber joints

The main components of this wall are the same as the ones used in the mortar joints wall. However, in this studied case there is a slightly difference in the disposition of the bricks and this wall also includes rubber joints between bricks and between the masonry and the columns of the reinforced concrete frame.

There are two versions of this wall: one with smooth horizontal deformable joints and another one in which the deformable joints were redesigned increasing the adherence of the surfaces in order to avoid a sliding effect in the interface between masonry and the deformable joints (Verlato et al., 2016). The first version is referred as DRES-V1 while the other one is called DRES-V2.

3.1.2.1. Reinforced concrete frame

The reinforced concrete frame of this model is exactly the same as the one built for the wall with mortar joints. The columns and beams have the same properties and dimensions and the reinforcement is placed in the same position.

The same reinforced concrete frame is used in both models (mortar joints and rubber joints) so that the different results obtained can be analysed. The variation of results should only be caused by the addition of rubber joints when studying this second model.

3.1.2.2. Mortar

Although now there are rubber joints inside the model, there is still mortar between most of the bricks of the infill and between the masonry and the beams of the reinforced concrete frame.

The same mortar is used for this case of study, which is class M 10.

3.1.2.3. Rubber

Rubber joints are the main difference between this model and the one previously explained. These joints are distinguished by having a low stiffness in the in-plane direction and a high stiffness all along the out-of-plane and vertical directions (INSYSME, 2013). The behaviour of rubber joints is governed by the properties of the rubber. The addition of rubber joints could be included in structures such as buildings based on reinforced concrete frames and located in regions where the intensity of earthquakes lies between medium and high (Calabria et al., 2016).

This experimental model includes three horizontal rubber joints inside the masonry infill with the purpose of reducing the damage in the infill because of the deformation of the frame during a seismic event. Not only has the model horizontal rubber joints but also vertical rubber joints between the infill and the columns of the reinforced concrete frame. These vertical rubber joints avoid having stress concentrations that might damage the columns of the frame as well as the masonry infill (INSYSME, 2013).
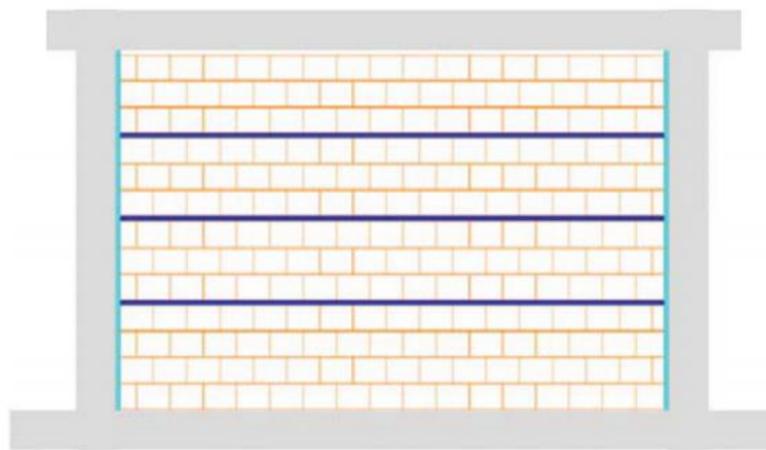
Figure 5. Distribution of rubber joints. Adapted from Calabria et al., (2016: p.1156).

3.1.2.4. Masonry infill

The same clay brick unit is used as the infill of the wall. However, the total number of brick rows is 13, instead of the 13.5 rows included in the mortar model. This is due to the addition of the three horizontal rubber joints that have a thickness and so the total height that the bricks have to cover is slightly reduced.

3.2. Loads

In the experimental model, not only was the out-of-plane load applied to the wall but also an in-plane load. Both loads represent the seismic action. However, there is also a third load applied in the top beam-column nodes. It is a vertical load that represents the action of upper floors in the reference building (Verlato et al., 2016).

The vertical load is constant and its value is 400 kN per node. The in-plane action is introduced applying a horizontal cyclic displacement in the top beam.

The procedure with which displacements are applied in the top beam for the in-plane test is quasi-static, with a maximum value of speed of 0.5mm/s. The test was carried out with 3 quasi-static cycles for every level of drift that was being studied. The drift (ψ) is the ratio between the inter-storey displacement and the height of the storey (Verlato et al., 2016). The different drift sequences that were tested are:

- +/-0.05, +/-0.1, +/-0.2, +/-0.3, +/-0.4, +/-0.5, +/-0.6, +/-0.8, +/-1.0, +/-1.2, +/-1.4, +/-1.6, +/-1.8, +/-2.0 and +/-2.4 (%)

Once the in-plane test is finished, the displacement is brought to zero and the out-of-plane test starts. The out-of-plane load is applied in 8 points located at the thirds of the length of the masonry wall and at the fifths of the height of the wall. These 8 points are symmetrically distributed in the wall (Verlato et al., 2016).
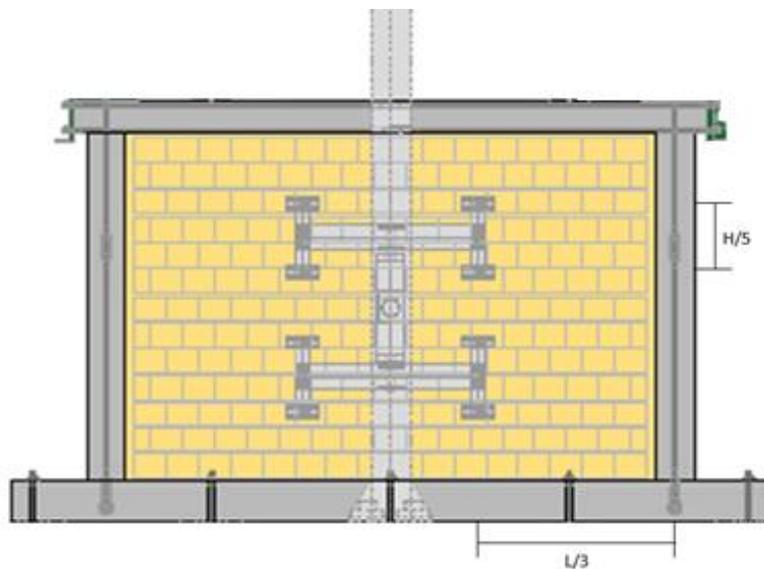
Figure 6. Application of out-of-plane loads. Adapted from Verlato et al., (2016: p.1361).

The out-of-plane load is applied in the eight points shown in Figure 6. It is increased until it reaches 60 kN. Once this value is reached, the load is brought back to zero and it is later increased in a monotonic way until reaching the ultimate displacement, which is a 20% of the maximum load decrease (Verlato et al., 2016).

3.3. Equipment

The experimental tests were carried out in a laboratory of the University of Padova, where the bottom beams of the masonry infill walls were bolted to the floor so that the base of the walls was fixed.

The vertical load is applied in the top beam-column nodes by means of an actuator located over the nodes. It is a self-locking device which is hinged to a beam made of steel located at

the top of this actuator. The steel beam is connected to the bottom beam of the reinforced concrete frame by ball and socket joints (Verlato et al., 2016).

In-plane loads are applied in negative and positive direction by means of a hydraulic actuator that introduces horizontal displacements in the node beam-column. The actuator is connected to a column made of steel that is bolted to the floor of the laboratory.

The out-of-plane loads are introduced on eight points by a hydraulic jack located in the centre on the structure.

In-plane and out-of-plane tests are not carried out at the same time. The setups for these tests are shown in Figures 7 and 8.
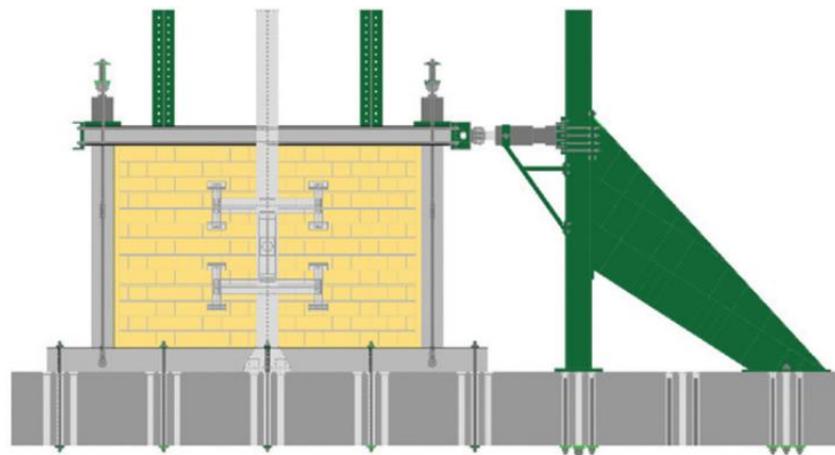
Figure 7. In-plane testing equipment (Verlato et al., 2016: p.1359).
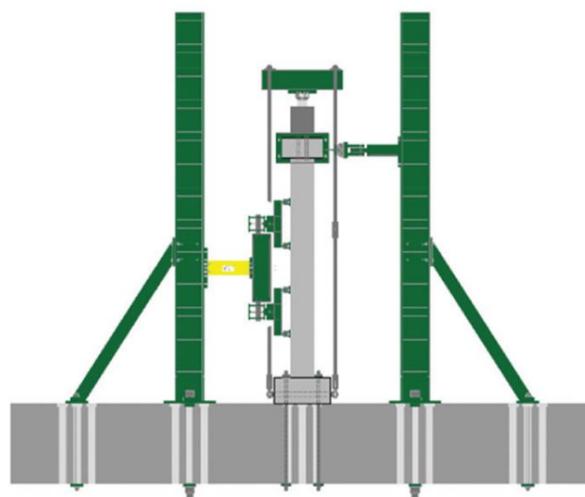
Figure 8. Out-of-plane testing equipment (Verlato et al., 2016: p.1359).

3.3.1. Instrumentation in the reinforced concrete frame

A total number of 19 instruments are introduced in the frame to measure displacements while the in-plane and out-of-plane tests are carried out.

In both top and bottom beams, a potentiometer and a MTS transducer are applied in order to measure the relative in plane displacement applied to the studied wall. Linear potentiometers are also applied between the top and bottom beams to quantify the inflection of the top beam of the frame. These potentiometers are located in the vertical direction.

Each column of the frame has three linear potentiometers applied in the horizontal direction so that their inflection can be measured.

While the frame was being built, six strain gauges were located in the bars of the longitudinal reinforcement, in the areas close to the nodes column-beam (Verlato et al., 2016).
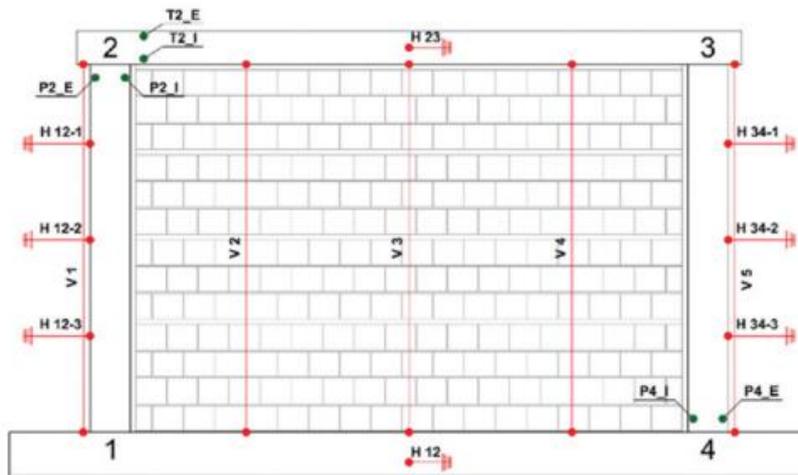
Figure 9. Distribution of the instrumentation in the frame (Verlato et al., 2016: p.1362).

In Figure 9 potentiometers are represented in red and the strain gauges in dark green.

3.3.2. Infill instrumentation for in-plane testing

Six instruments are used for the in-plane testing. These instruments are linear and draw wire potentiometers. Two linear potentiometers are located in the vertical direction, two of the four draw wire potentiometers in the horizontal direction and the other two in the diagonal direction. Potentiometers create a rectangle with two diagonals in the infill (Verlato et al., 2016).

The wall with rubber joints includes 11 additional potentiometers: 8 located between the columns of the frame and the masonry infill and 3 in the middle of each of the horizontal rubber joints. The eight potentiometers between columns and infill are located upon every row of bricks which is in contact with a rubber joint.
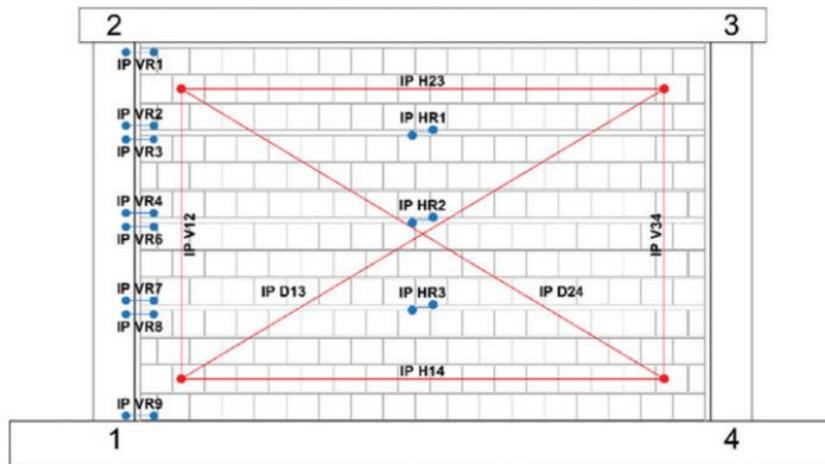
Figure 10. Instrumentation for the in-plane testing (Verlato et al., 2016: p.1362).

In Figure 10 the 6 potentiometers used for in-plane testing of walls with mortar joints are shown in red and the additional 11 potentiometers for rubber joints walls are represented in blue.

3.3.3. Infill instrumentation for out-of-plane testing

Instrumentation is distributed in the infill so that it can capture the global deflection of the infill wall in the out-of-plane direction.

For the wall with only mortar joints, a total amount of 15 draw wire and linear potentiometers are located in the infill wall. This out-of-plane instrumentation is distributed in the horizontal centre line of the wall as well as in the vertical direction at the thirds of the width of the wall, where the out-of-plane loads are applied.

The wall that includes rubber joints has two additional draw-wire potentiometers and three linear potentiometers. Draw-wire potentiometers capture the out-of-plane shear deformation of the lowest rubber joint inside the infill whereas the three linear potentiometers are located in each rubber joint between bricks in order to record the compressive deformation (Verlato et al., 2016).
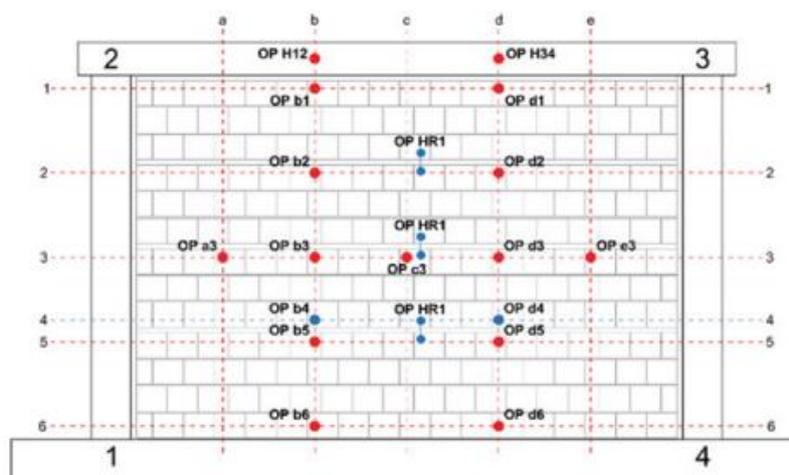
Figure 11. Instrumentation for out-of-plane testing (Verlato et al., 2016: p.1362).

Figure 11 shows the distribution of the potentiometers for the wall with mortar joints (red) and the additional instrumentation included in the wall with rubber joint (blue).

3.4. Results

Results have been obtained for both in-plane and out-of-plane tests. It must be taken into account that there are no results for only out-of-plane loads as these loads were applied after the enclosures were damaged due to previous in-plane testing. Out-of-plane loads were never applied directly on an undamaged wall.

3.4.1. In-plane test

The results obtained after carrying the in-plane tests are shown in the following graphs. These graphs collect both the hysteretic loops as well as the envelope curves which refer to the three cycles of the in-plane tests. The in-plane test was carried out in three different walls:

- Masonry infill wall with mortar joints (FC.MJ)
- Masonry infill wall with DRES-V1 rubber joints (FU.R1)
- Masonry infill wall with DRES-V2 rubber joints (FU.R2)
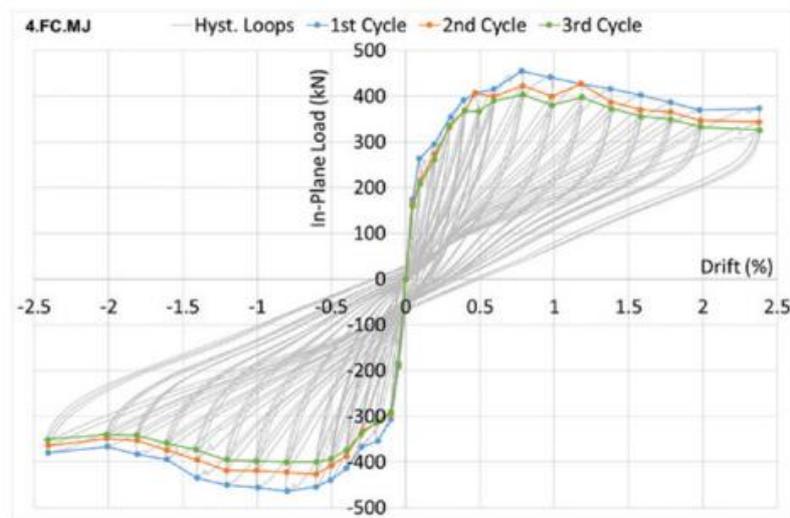
Figure 12. Envelope curves of in-plane test on FC.MJ (Verlato et al., 2016).

Figure 12 shows the envelope curves obtained after developing the in-plane test on the masonry infill wall with mortar joints. The results show a high stiffness during the beginning of the test. However, stiffness starts decreasing from the 0.1% drift and the maximum strength was reached at the 0.8% drift. Once this maximum strength was reached, the in-plane load decreased until the test finished. This is because of the development of diagonal cracks during the in-plane test, which diminishes the infill's stiffness. At 2.4% drift, not only diagonal cracks appeared in the wall but also several masonry bricks crushed in column-beam nodes (Verlato et al., 2016).
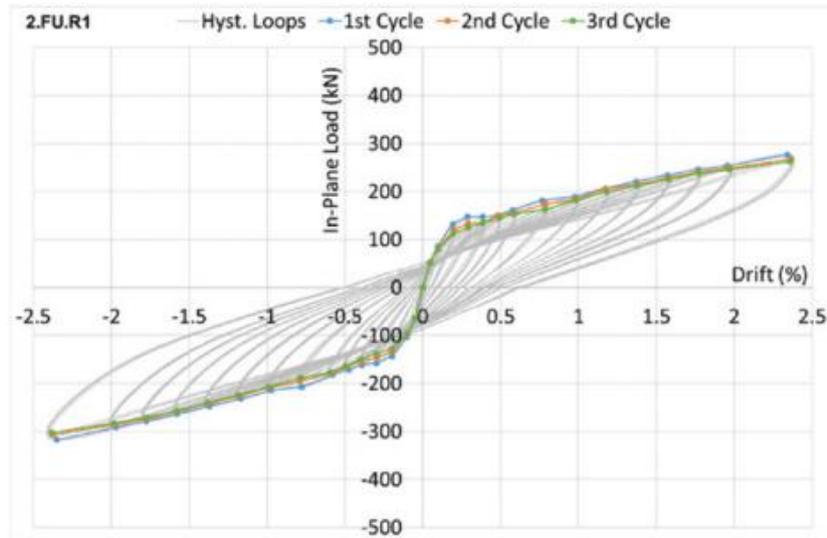
Figure 13. Envelope curves of in-plane test on FU.R1 (Verlato et al., 2016).

In Figure 13, the envelope curves obtained after developing the in-plane test in the masonry infill wall with rubber DRESS-V1 joints are shown. Compared to the results obtained for the FC.MJ enclosure, the shape of the envelope curves is clearly more elliptical. Until a 0.2% drift, the behaviour that the enclosure is quite regular. However, after that point, it quickly starts loosing stiffness. This behaviour is caused by the activation of the sliding effect along the mortar and deformable joints interfaces. The maximum strength in the in-plane direction was not reached by the enclosure by the end of the test (2.4% drift). Thanks to the horizontal sliding effect, the damage in the infill was limited. However, as some rows of bricks slid along the deformable joints, permanent deformations appeared in the wall at the end of the test. (Verlato et al., 2016).
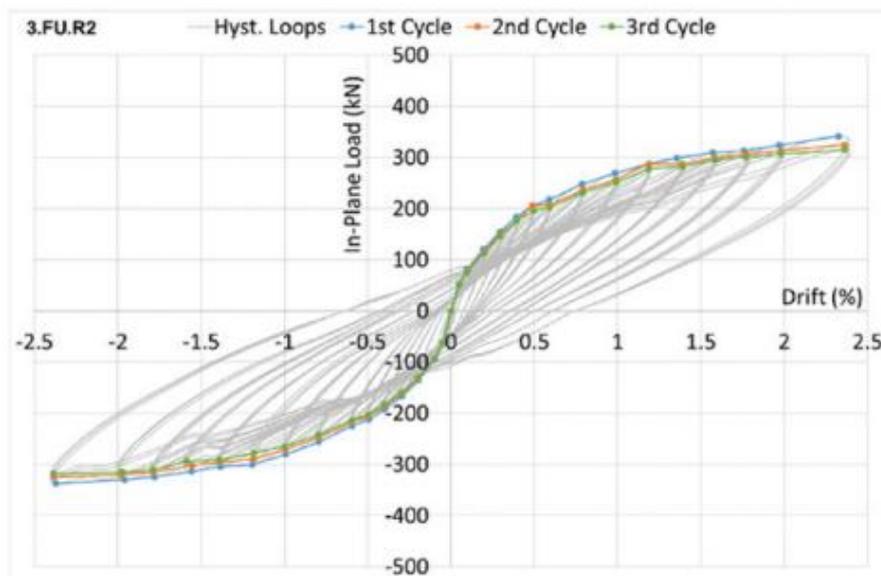
Figure 14. Envelope curves of in-plane test on FU.R2 (Verlato et al., 2016).

The last in-plane test was carried out in a masonry infill wall with rubber DRES-V2 joints, and the results obtained for this test are shown in Figure 14. These joints are distinguished by having an improved adherence compared to the DRES-V1 joints. They prevented the development of the sliding effect along the interfaces of masonry and deformable joints, and so the behaviour of the enclosure is more regular than for the previous case with DRES-V1 joints. Stiffness decreases gradually and thanks to the improved adherence of the joints, permanent deformations were prevented at the end of the test. Avoiding these permanent deformations implied the formation of some diagonal cracks near the columns of the frame, but the damaged part of the structure was clearly reduced compared to the FC.MJ enclosure (Verlato et al., 2016).

Figure 15. Left to right, FU.R2 and FC.MJ frames after in-plane test (Verlato et al., 2016).

As well as it happened with the FU.R1 enclosure, the maximum in-plane strength was not reached once the test finished at 2.4% drift.

It is also interesting to compare the results obtained for one same cycle for the three different masonry infill walls tested, so that some conclusions can be made. During the experiment carried out in the University of Padova, not only the three different walls mentioned were tested (FC.MJ, FU.R1 and FU.R2) but also a bare frame without masonry infill. After obtaining the in-plane results, it was possible to obtain the infill contribution by subtracting to each envelope curves of the walls the load contribution of the bare frame (Verlato et al., 2016).
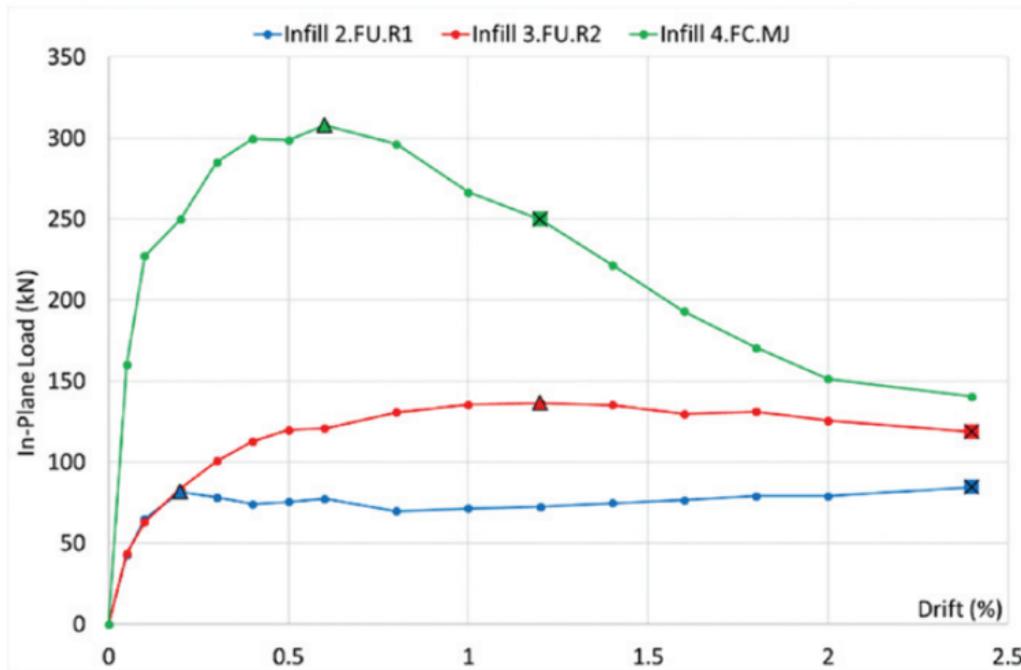
Figure 16. Infill contribution in the in-plane tests (Verlato et al., 2016).

Figure 16 shows the results of the infill contribution during the third cycle carried out in the in-plane tests. Triangles show the maximum infill contribution and squares highlight the ultimate infill strength, considered as the 80% of the maximum strength.

The contribution of the infill in the masonry wall with mortar joints (FC.MJ) is the highest when it comes to maximum load, as the maximum strength is reached in this enclosure (308 kN). However, once this value is reached, the contribution of the masonry infill starts decreasing until the end of the test (Verlato et al., 2016).

The infill contribution of the wall with rubber DRES-V2 joints (FU.R2) demonstrated a more regular behaviour, being the maximum strength reached at 1.2% drift. After this point, it starts decreasing gradually until the end of the test at 2.4% drift. The main difference with the FC.MJ wall is that, by the end of the test, the infill of the FU.R2 wall decreased its contribution by a 20% whereas in the FC.MJ wall, the infill contribution decreased more than 50% by the end of the in-plane test (Verlato et al., 2016).

Maximum Infill Contribution		
Wall	Fmax (kN)	Drift (%)
FC.MJ	308	0.6
FU.R1	82	0.2
FU.R2	136	1.2

Table 1. Maximum infill contribution during in-plane test.

By introducing the rubber DRES-V1 joints in the infill enclosure, the damage of the infill during deformations in the in-plane direction, was reduced. This is because of the inclusion of the rubber joints that allowed the masonry brick rows slid along the deformable joints. However, this implied a reduction in the stiffness of the infill and permanent deformations were introduced in the structure after the in-plane displacements (Verlato et al., 2016).

New deformable joints were introduced in the model to avoid the sliding effect between bricks and the previous DRES-V1 deformable joints. These new joints are the DRES-V2 system and with them an optimisation of the interaction between the frame and the enclosure was achieved. Thanks to these joints, the damage in the masonry was reduced compared to the FC.MJ wall, achieving an optimal behaviour in the in-plane direction (Verlato et al., 2016).

The following figures show the improved behaviour of the masonry infill wall against in-plane loading once the deformable rubber joints were introduced. The pictures include half wall with mortar joints (MJ) and half wall with rubber joints (RJ).
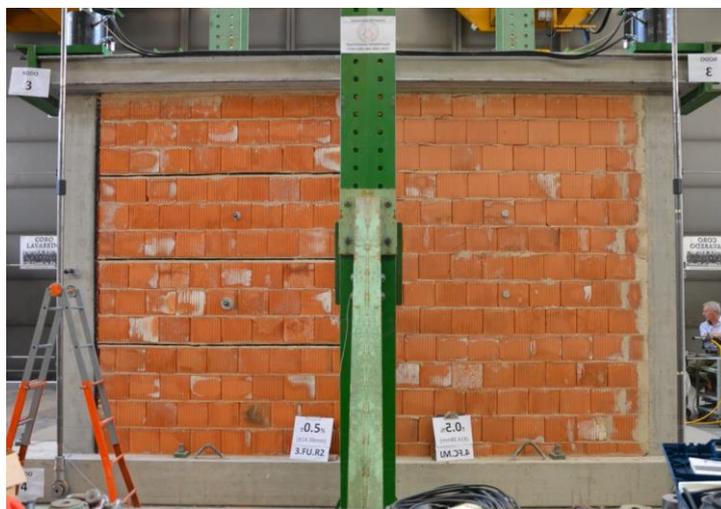
Figure 17. Behaviour of RJ and MJ walls during in plane test at 0.5% drift (INSYSME, 2013).

Figure 18. Behaviour of RJ and MJ walls during in plane test at 1.2% drift (INSYSME, 2013).

Figure 19. Behaviour of RJ and MJ walls during in plane test at 2.4% drift (INSYSME, 2013).

From Figures 17 to 19 it can be observed that the damage in the infill increases with the % of drift and that more cracks appear. However, it is important to say that the masonry infill with mortar joints clearly shows more damage than the one with rubber joints. For instance, in Figure 19, the upper right node column-beam has been damaged after the in-plane test, with the resulting crushing of some bricks. There are also diagonal cracks, being the largest one close to the centre of the wall. Nevertheless, on the left, the wall with rubber joints does not show damaged bricks and the length of the cracks is considerably reduced.

3.4.2. Out-of-plane test

It must be considered that the out-of-plane tests were carried out after the in-plane tests, which means that the results obtained for the out-of-plane testing include previous in-plane damage.

Three different walls were studied: wall with mortar joints, wall with DRES-V1 rubber joints and wall with DRES-V2 rubber joints. In the case of the two walls with rubber joints, these joints were identically distributed in both models. The results obtained are shown in Figure 20.
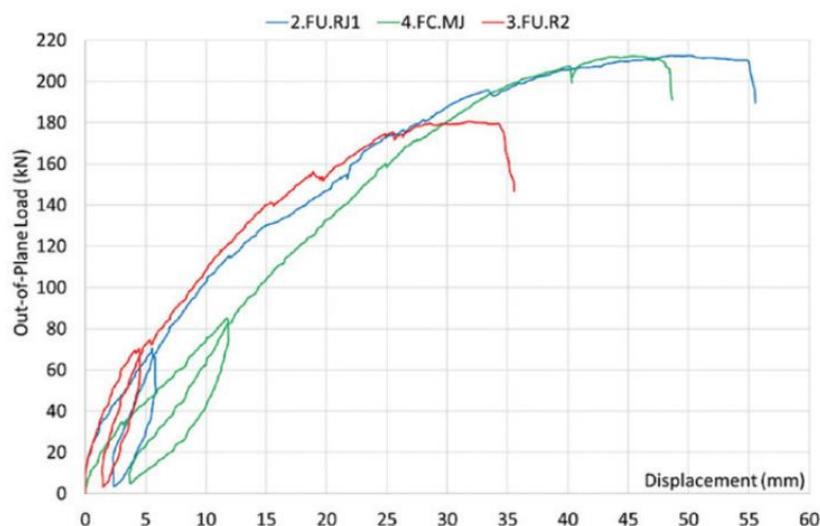
Figure 20. Out-of-plane results of the experimental models (Verlato et al., 2016: p.1365).

The same three walls studied for the in-plane test where later studied considering out-of-plane loads:

- FU.R1 refers to masonry infill wall with DRES-V1 rubber joints
- FC.MJ refers to masonry infill wall with mortar joints
- FU.R2 refers to masonry infill wall with DRES-V2 rubber joints

These results were obtained with out-of-plane tests which were carried out in the walls with an in-plane damage at a drift value of 2.4% associated to the Ultima Limit States (INSYSME, 2013).

Maximum loads - Displacements		
Wall	Fmax (kN)	Displacement (mm)
FC.MJ	212	45.5
FU.R1	213	48.6
FU.R2	181	31.8

Table 2. Maximum loads obtained and the associated displacements for out-of-plane test.

In terms of the maximum forces obtained for each wall, the results are quite similar, not having a big difference between the three values. However, it can be noticed that the wall with DRES-V1 rubber joints (FU.R1) reached the highest value of strength, 213 kN, whereas the wall with DRES-V2 rubber joints (FU.R2) reached 181 kN.

Both FU.R1 and FU.R2 showed a higher initial stiffness compared to the FC.MJ wall without rubber joints. Not only does the introduction of rubber joints increase the maximum stiffness but also the maximum strength in the out-of-plane direction. These rubber joints prevent the damage of the brick rows (Verlato et al., 2016).

The reason why the FC.MJ wall was able to reach a maximum load of 212 kN during the out-of-plane test after being damaged with an in-plane test is because, the main damage that the masonry suffered with the in-plane test, was located in the areas close to the beam-column nodes, while the out-of-plane loads are applied in the central area of the masonry wall. However, the wall experienced several damage that includes the expulsion of bricks.

When it comes to displacements, the maximum values registered and their respective loads are collected in Table 3.

Maximum displacements - Loads		
Wall	Fu (kN)	Displacement (mm)
FC.MJ	191	48.6
FU.R1	190	55.5
FU.R2	147	35.5

Table 3. Maximum displacements and their associated loads for out-of-plane test.

Figure 21. Deformation of the experimental wall with rubber joints (LATERIZIO, n.d.).

Figure 21 shows the deformed shape and the cracks that appeared in the experimental model of a masonry infill wall with rubber joints after the out-of-plane loads were applied. The shape of the crack forms a cross, which is the characteristic affection that structures experience during a seismic event.

The inclusion of rubber DRES-V2 joints in the enclosure implied not only an improved behaviour in the in-plane direction but also a better performance in the out-of-plane direction. The initial strength and stiffness of the enclosure were outstanding.

4. NUMERICAL MODELS

After the development of the experimental models, several researchers decided to develop numerical models based on the dimensions and properties of the structures used in the University of Padova, in order to recreate those models and study how realistic the results obtained could be (Calabria et al., 2016).

In this project, numerical models are developed to recreate the experimental models and based in two different approaches: macro and mesoscales. Inside each approach, a wall with mortar joints and another one with rubber joints are created. Although the experimental tests were carried out considering two different rubber joints (DRES-V1 and DRES-V2), only one rubber numerical model is developed in order to study the efficiency of those joints. Both macro and mesoscale models are created with the software Abaqus.

4.1. Macroscale models

Macroscale models are characterised by being a simplification of real models. These kinds of models are easier to implement and run as they are not defined in such detail. The main purpose of these models consists of simulating the general response of a structure, not being

able to predict a detailed behaviour of the different elements of the structure (Camacho & Hallett, 2015).

Nevertheless, macroscale models do allow to study the benefits of the addition of rubber joints inside masonry infill walls. Despite not being the most accurate representation of reality, they still show the main differences between walls with and without rubber joints when out-of-plane loads are acting on them, so that is the main reason why the development of these models is part of the scope of the project.

4.1.1. Wall with mortar joints

In order to develop the model, the main elements of the wall need to be introduced. This means defining the dimensions as well as the properties of the different materials. Properties are introduced in the software as accurate as possible, trying to replicate the properties of the materials used in the experimental models.

4.1.1.1. Structure

3.1.1.1.1. Reinforced concrete frame

In order to create the structure of the frame, both concrete and reinforcement elements need to be defined. It is important to take into account that the steel elements are created separately from concrete elements, which means that bars an stirrups are created independently. Once the steel elements are defined, they are located in their final position inside the concrete beams and columns and they are bond to the concrete solids in order to ensure that both work as a unique structure, making sure that the loads and stresses are properly transmitted.

Regarding the concrete elements of the wall, two columns and two beams need to be defined. All elements are defined as *Parts* inside the software and, if two *Parts* have the same properties and characteristics, it is not necessary to introduce two different *Parts* but only one which will be replicated when necessary. This means that three *Parts* were defined for the concrete wall: bottom beam, top beam and column.

All concrete *Parts* are created as solids inside the software. The height and width of column and beams are introduced, and, after that, the depth is obtained by extrusion of the cross section of each *Part*. The three *Parts* are created, but they are not located in their final position. They will be organised once the assembly step is reached.

The elements are created but they do not have any material properties. In order to assign a material to these solids, the material concrete has to be created. Abaqus asks for several parameters of the material, which are introduced as similar as possible as the properties of the concrete used in the experimental models. The properties introduced for concrete are shown in the Table 4.

Concrete properties	
Young's Modulus (E)	22 GPa
Poisson's ratio (v)	0.15
Fracture Energy (Gf)	0.075 N/mm
Yield Stress (ft)	3.9 MPa

Table 4. Concrete properties introduced in the numerical model.

The contact surfaces between beams and columns are defined as partition planes so that the future mesh of the structure does coincide with these surfaces.
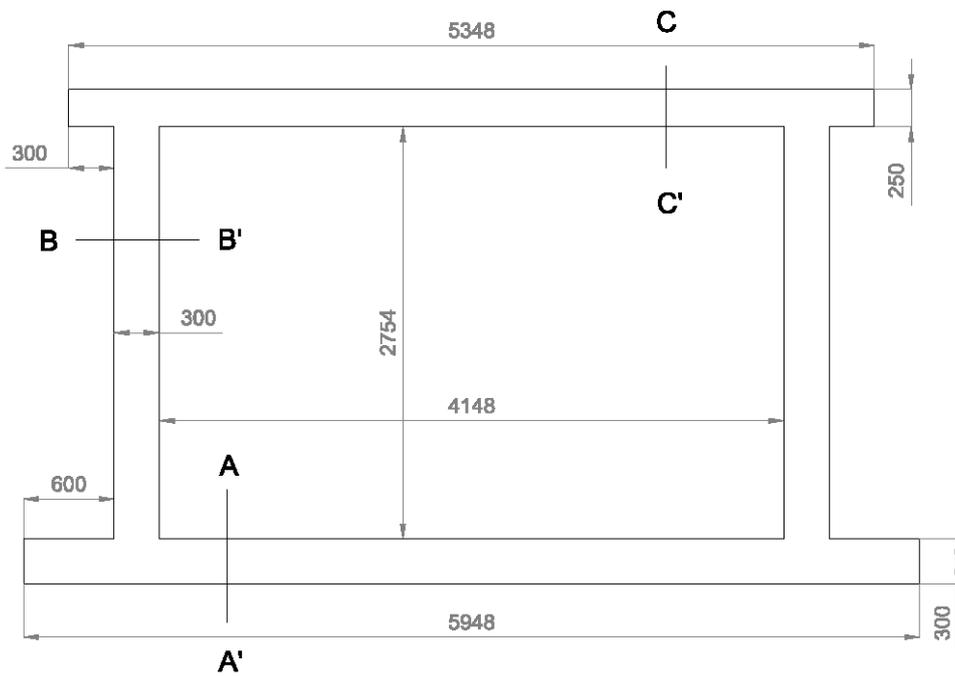
Figure 22. Wall dimensions for the numerical models. Dimensions in mm.
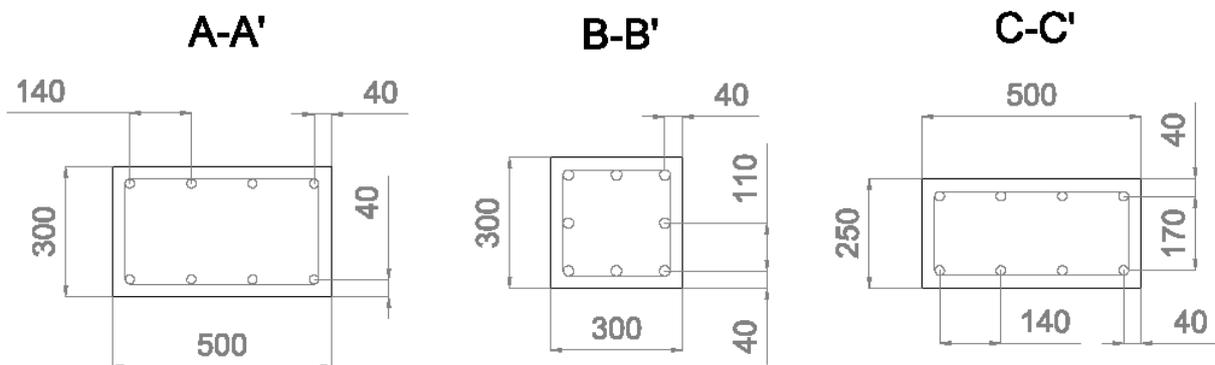
Figure 23. Cross sections of beams and columns. Dimensions in mm.

Once concrete elements are fully defined, rebars and stirrups need to be introduced in the model. Instead of creating a *Part* for each bar or stirrup, only one is created for every element that appears more than once in the model, and it will be replicated later. The total steel *Parts* created are:

- Columns:
    - Bars of Φ22
    - Stirrups of Φ8
    - Stirrups of Φ10
- Beams:
    - Bars of Φ22
    - Stirrups of Φ8

There are Φ8 stirrups in both beams and columns, so only one stirrup with a diameter of 8 mm is created and then replicated in order to introduce it inside both solids.
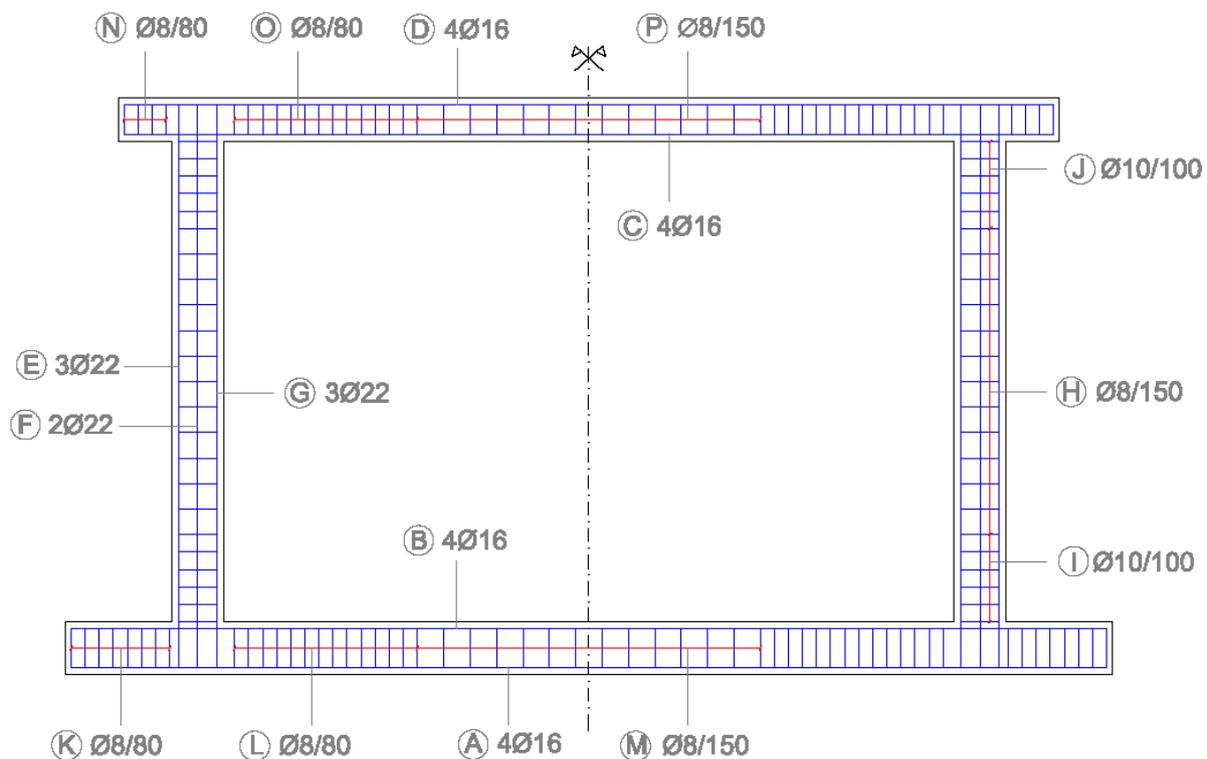
Figure 24. Distribution of the reinforcement in the numerical models.

The reinforcement elements are not introduced as solid *Parts* but as wire elements. This means that they do not have any depth and, apart from assigning the material, a cross section must be assigned to each of them. Introducing the reinforcement as wire elements implies drawing lines with the length and shape requires.

As it happened with the concrete, now the material steel needs to be introduced inside the software so that it can later be assigned to all the reinforcement elements created. The properties of this material are shown in Table 5.

Steel properties	
Young's Modulus (E)	144 GPa
Poisson's ratio (v)	0.3
Fracture Energy (Gf)	-
Yield Stress (ft)	530 MPa

Table 5. Steel properties introduced in the numerical models.

When it comes to the cross section of the steel elements, four different diameters are introduced in the software: 8,10, 16 and 22 mm. These diameters are assigned to each steel *Part* created, so that bars and stirrups have material properties and the correct dimensions.

As the different elements of the reinforced concrete frame are created, it is time to assembly the structure.

The *Parts* that appear more than once are replicated and each *Part* is located in the place where it is supposed to be. As the reinforcement elements are inside the concrete solids, they can not be observed unless the concrete beams and columns are suppressed.

Although all the concrete solid elements are now together and located in their final position, they are still acting individually. It is important to define the concrete frame as a unique structure, not as a structure based on four different elements that are not connected. In order to ensure that all four concrete parts are working together, they are selected and merged, creating the concrete frame.

Figure 25. Reinforced concrete frame.

As it has been mentioned before, bars and stirrups are inside the merged concrete frame, but they are not interacting yet with the frame. In order to let the software understand that the reinforcement elements need to be connected to the concrete frame, a *Constraint* has to be created. Steel elements are selected and then it is said as a constraint that they are inside the merged concrete frame. Thanks to this option, the software understands that the loads acting on the surface of a concrete element are transferred to the reinforcement elements inside.

3.1.1.1.2. Masonry infill

As the model that is being developed is a macroscale model, the masonry infill will not be created as several bricks but as a big plate which will be assigned with the masonry properties. This means that this *Part* is created as a solid.

This big plate has the same depth as the columns, which is 300 mm. Depth is assigned to the element by using the extrude option. As well as with the concrete and reinforcement *Parts* introduced in the model, a new material has to be defined so that the masonry properties can be assigned to the plate. The masonry properties introduced in Abaqus are shown in Table 6:

Masonry properties	
Young's Modulus (E)	1.5 GPa
Poisson's ratio (v)	0.4
Fracture Energy (Gf)	0.04 N/mm
Yield Stress (ft)	0.18 MPa

Table 6. Masonry properties of the numerical models.

Once this *Part* is assigned with the properties shown in Table 6, the masonry infill is represented in the model. However, it must be noticed that, as there are no contact surfaces between bricks, once the model is tested, no cracks will appear following these contact surfaces. The response of the macroscale model will not be exactly the same as the response obtained from the experimental model.

As the concrete frame is already merged, once the masonry infill is defined as a *Part* it is located in its final position inside the frame. The main structure of the model is now created and the only elements missing for this model are the mortar interactions between the masonry infill and the frame.

3.1.1.1.3. Mortar

There are only mortar joints in this model, so the only material that needs to be introduced in the software.

Regarding the experimental model, the mortar used was class M 10 and it was located between bricks and between the masonry infill and the concrete frame. In this case, there are no bricks in the model as the masonry infill is included as one big element, which means that mortar only needs to be introduced in the contact surfaces between frame and the masonry *Part.*

In the numerical model, mortar is not introduced as a material with a thickness. Instead, the contact surfaces of the elements in which there is mortar, are assigned with interaction properties that represent the action of the mortar. This is the main difference between experimental and numerical models. What is more, mortar interaction properties are not the same for the contact surfaces of the masonry infill-columns and for the surfaces between masonry infill-beams. These interaction properties are obtained after Calabria et al., (2016) and the characteristics are shown in Tables 7 and 8:

Mortar - Beam interaction	
Normal Stiffness (Kn)	50 N/mm^3
Shear Stiffness (Ks)	25 N/mm^3
Coefficient of friction (tanφ)	0.031 N/mm

Table 7. Mortar - Beam interaction properties.

Mortar - Column interaction	
Normal Stiffness (Kn)	1000 N/mm^3
Shear Stiffness (Ks)	500 N/mm^3
Coefficient of friction (tanφ)	0.031 N/mm

Table 8. Mortar - Column interaction properties.

Once mortar is defined as an interaction property, it has to be introduced in the contact surfaces between the masonry plate and the concrete frame. In order to do so, the main structure needs to be defined so that the software is able to find contact surfaces between *Parts.* As the concrete frame has already been merged together, there are no contact surfaces between beams and columns. For this studied model, only four contact surfaces are identified: 2 between the masonry infill and the beams and 2 between the masonry infill and the columns. They are assigned with the corresponding interaction properties.

The whole macroscale structure with mortar joints is created and now the different loads have to be introduced as well as the boundary conditions.

4.1.1.2. Loads

The different loads considered in the model are the following ones: gravity, vertical load and out-of-plane load.

Both gravity and vertical loads are introduced as static loads. Gravity acts upon al the structure but the vertical load in only applied in the top of the columns, as in the experimental model. This load represents the action of possible storeys of a building and it is introduced as a pressure load, being its value 4.4 N/mm^2.

When it comes to out-of-plane loads, they are not introduced as static but dynamic loads. In order to introduce these loads in the model, the first step consists of defining the points in which they are going to be applied.

Following the experimental model, the out-of-plane load is applied in 8 different points located in the masonry infill. However, in order to introduce the loads in the model, the different points should be defined. These points are attached to the different surfaces of the structure and the loads are introduced acting on them. This is how the software understands that the loads applied are acting on the different surfaces of the wall.

For the out-of plane loads, eight *Reference Points* are introduced in the masonry infill. These points are located at the thirds of the length of the wall and at the fifths of the height. As a result, there are two columns of 4 *Reference Points* on each. Apart from these eight points, another *Reference Point* is created and located in the centre of the wall so that the displacements can be measured on it, in the centre of the structure.
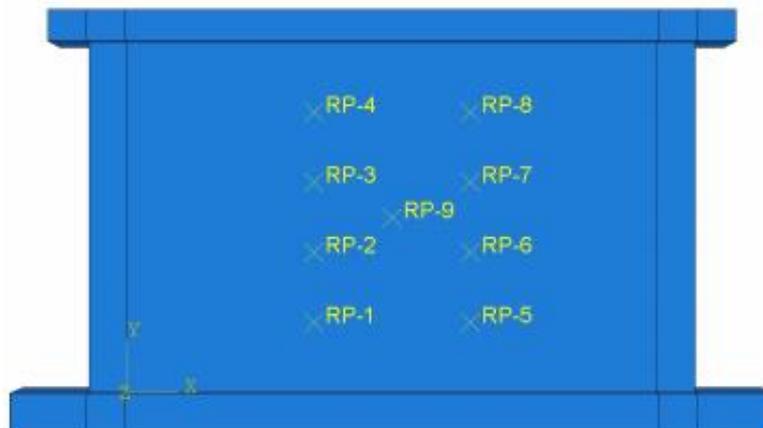
Figure 26. Macroscale mortar model.

Once the points in which loads are acting are defined, loads can be introduced in the model. As dynamic loads, out-of-plane loads are created as monotonic loads with displacement control. This means that instead of introducing a load, an incremental displacement is assigned to each *Reference Point* so that the force can be obtained from the displacements. The displacement for the out-of-plane loads is perpendicular to the wall. While gravity and vertical loads are introduced inside the model as *Loads*, monotonic loads with displacement control are introduced as *Boundary Conditions*.

Loads are applied in *Sets*, which means that not all the forces are acting at the same time. First the gravity load, then the vertical loads acting on the column. Once these static loads are applied, the out-of-plane loads are introduced as *Boundary Conditions*. This process is carried out in a total of three *Sets*, in which each *Set* includes a load.

4.1.1.3. Boundary conditions

In order to recreate the same conditions as in the experimental models, two boundary conditions are defined in the numerical models.

The bottom beam is clamped so that there are no displacements nor rotations on it and the back surface of the top beam is pinned.
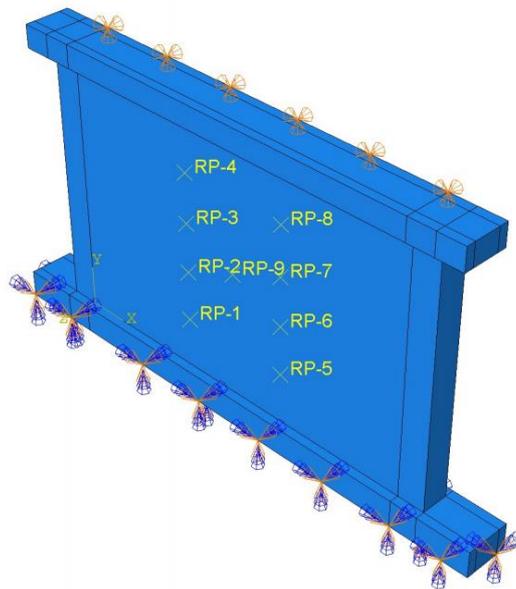
Figure 27. Boundary conditions.

Once the loads and boundary conditions are defined in the model, each of the different parts of the structure needs to be meshed so that the displacement results are obtained as accurate as possible. The smaller the mesh, the longer it takes to obtain the results.
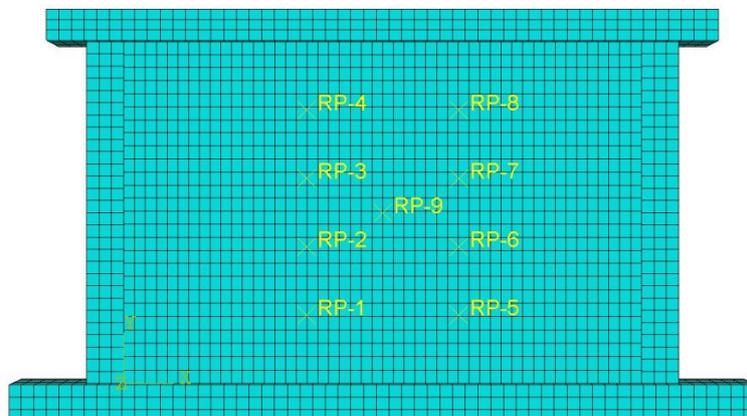
Figure 28. Distribution of the mesh in the numerical model.

4.1.2. Wall with rubber joints

Inside macroscale models, a wall with rubber joints was developed in order to compare the results obtained with the previous wall model in which there are only mortar joints. This model includes three horizontal rubber joints as well as two vertical ones between the masonry infill and the columns of the reinforced concrete frame.

4.1.2.1. Structure

Not all the different elements of the structure are modelled in the same way as in the previous macroscale model with mortar joints. The main difference lies on the masonry plate as well as introducing a new interaction property, which is the rubber.

4.1.2.1.1. Reinforced concrete frame

The reinforced concrete frame used in this model is exactly the same as the one used for the wall with mortar joints. There is no difference in the materials nor in the dimensions of the columns and beams so that both models can be compared.

4.1.2.1.2. Masonry infill

It is not possible to define the masonry infill as a big plate because three horizontal rubber joints have to be introduced between the bricks in order to recreate the experimental model carried out in the University of Padova.

As there are three horizontal rubber joints, the masonry infill is divided into four parts. So for this model, instead of defining one big masonry plate, four smaller plates will be introduced on the software. Three of them have the same dimensions and the fourth one is slightly bigger, located in the bottom. As there are three equal plates, only one *Part* is defined for them and then it is replicated two times.

Once the plates are created, they are assigned with the masonry properties. They are then located in their final positions, once above another. By creating these four masonry plates, there are a total of 7 interaction surfaces: 4 between plates and frame and 3 between the plates themselves.
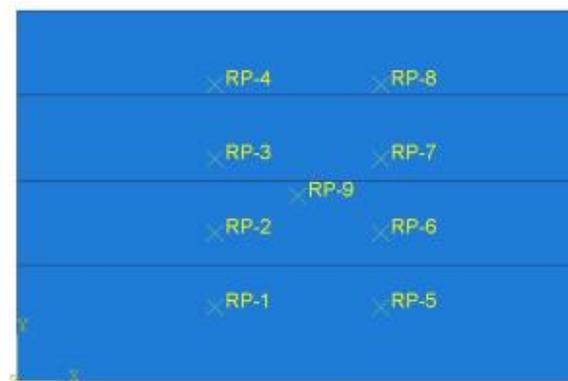
Figure 29. Masonry infill for the macroscale model with rubber joints.
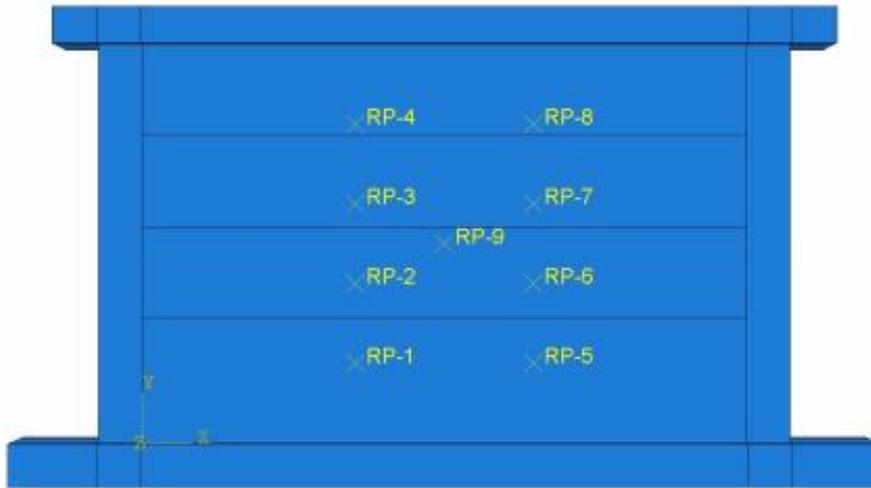
Figure 30. Macroscale model of wall with rubber joints.

4.1.2.1.3. Mortar

Mortar interaction properties are assigned between the beams of the reinforced concrete frame and the masonry plates. Again, mortar is not introduced as a material but as an interaction between surfaces.

4.1.2.1.4. Rubber

In the experimental models rubber was introduced as a material with a thickness. However, in the numerical models carried out for this project, rubber is introduced as an interaction property between the different contact surfaces.

Two different interaction properties are defined in the model: one for the rubber joints between the masonry walls and another one for the rubber joints located between the masonry plates and the reinforced concrete columns of the frame. The properties of both joints are shown in the following tables:

Rubber - Column interaction	
Normal Stiffness (Kn)	10 N/mm^3
Shear Stiffness (Ks)	0 N/mm^3
Coefficient of friction (tanφ)	-

Table 9. Rubber - Column interaction properties.

Rubber - Infill interaction	
Normal Stiffness (Kn)	10000 N/mm^3
Shear Stiffness (Ks)	500 N/mm^3
Coefficient of friction (tanφ)	0.4

Table 10. Rubber - Infill interaction properties.

4.1.2.2. Loads

The loads acting on this model are exactly the same as the ones introduced in the mortar wall: gravity, vertical load on the top of the columns and out-of-plane loads acting on the masonry infill. As there is more than one masonry plate, the *Reference Points* in which the out-of-plane loads are applied are distributed between the four masonry plates.

Again, three steps are defined in order to introduce the loads in the model. The out-of-plane load starts acting once the vertical load has been applied.

4.1.2.3. Boundary conditions

The bottom beam of the reinforced concrete frame is clamped whereas the back surface of the top beam is pinned, approximating the boundary conditions to the ones established in the laboratory while developing the experimental models.

4.2. Mesoscale models

Not only two macroscale models are developed in this project but also two mesoscale models. Mesoscale models are an accurate representation of the experimental models. In these models, each of the bricks that are part of the masonry infill are defined one by one. This means that the structure is more similar to the experimental one so the expected response of the wall will be analogous.

Apart from comparing the rubber and mortar mesoscale models, by creating them it is possible to see if these numerical models are actually representing the real behaviour of a masonry infill wall. It takes longer to run the models and obtain the results due to the level of detail in which the structure is created.

As the main difference between mesoscale and macroscale models relies on the structure of the wall itself, boundary conditions will not be explained for the mesoscale models as they are the same than for the macroscale models.

Regarding loads, the main difference with macroscale models is that, for mesoscale models, there is also an in-plane load acting on the wall. This in-plane load is applied in a new *Reference Point* which is located in the lateral surface of the top beam. It is also introduced

as a monotonic load with displacement control. This means that there will be a total of four *Sets* for the mesoscale models, one per load. The in-plane load acts after the vertical load has been introduced and before the out-of-plane load starts acting. This implies that, as well as in the experimental models, the out-of-plane load starts acting on the wall after being damaged by an in-plane load. The *Reference Points* in which out-of-plane loads are applied, are now set in different bricks, not in one same plate as it happened with the macroscale models.

4.2.1. Wall with mortar joints

This is a similar model to the one created in macroscale, with the difference of the masonry infill which is introduced defining all the bricks of the structure.

4.2.1.1. Reinforced concrete frame

The reinforced concrete frame is the same during the whole process of modelling the masonry infill wall.

4.2.1.2. Masonry infill

Inside the software Abaqus, instead of creating a masonry plate, a new *Part* has to be created for the mesoscale models. This new *Part* represents a brick and it is a cube of 244x204x300 mm^3 which is defined in the model as a solid element. Only one brick unit was used in the experimental models, and this unit was adapted to the frame. This means that in some rows of bricks, there were bricks cut in half so that they fitted the frame. However, inside the software, if there is a brick with half of the width or half of the height, a new solid element has to be created so that it represents this modified brick.

For the wall with mortar joints developed in the experimental model, there were a total of 13.5 rows of bricks. The first row was formed by bricks which had half of the height of the base brick unit. Apart from that, there were some bricks in contact with the columns of the frame that had half of the width. This means that in order to reproduce the same model in Abaqus, four different brick units have to be defined:

- One brick unit of 244x204x300 mm^3
- Brick with half height 244x102x300 mm^3
- Brick with half width 122x204x300 mm^3
- Brick with half width and half height 122x102x300 mm^3

The last brick with half width and half height is located in the corner of the first row of bricks, between the bottom beam and the columns.

Once the four *Parts* are created in the model, they are assigned with the masonry properties, which are the same for all the units of bricks defined. Masonry properties are the same as the ones assigned to the plates in the macroscale models.

As the reinforced concrete frame has already been defined, bricks need to be included inside the frame. The four bricks are introduced in their position inside the frame and then they are replicated until the whole masonry infill is defined. The same number of rows are created, 13.5 where the first row of bricks has half of the height.
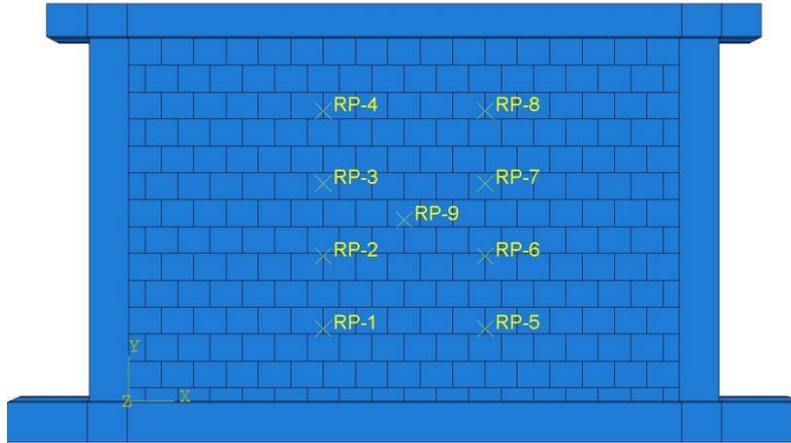
Figure 31. Mesoscale model with mortar joints.

4.2.1.3.   Mortar

As it has been explained, neither mortar nor rubber are introduced inside the numerical models as materials but as interaction properties between the different contact surfaces.

For the mesoscale mortar model, the interactions between bricks and beams and bricks and columns have the same properties as for the macroscale models, being these properties collected in Tables 7 and 8.

However, as there are now brick units, the contact surfaces between them have to be assigned with interaction properties as well. These interaction properties are not the same as the ones between masonry and frame, and they are included in Table 11.

Masonry interaction	
Normal Stiffness (Kn)	500 N/mm^3
Shear Stiffness (Ks)	250 N/mm^3
Coefficient of friction (tanφ)	0.4

Table 11. Masonry interaction properties.

4.2.2. Wall with rubber joints

This mesoscale model includes three horizontal rubber joints as well as two vertical rubber joints between the masonry infill and the columns of the reinforced concrete frame.

4.2.2.1. Reinforced concrete frame

The same reinforced concrete frame is defined for this model, having the beams and columns merged together and with one *Reference Point* attached to one lateral surface of the top beam so that the in-plane load can be applied on it.

4.2.2.2. Masonry infill

While developing the experimental model of the masonry infill wall with rubber joints, the total number of rows of bricks was established in 13 instead of 13.5 as three horizontal rubber layers with a thickness were introduced in between the bricks, so the total height to cover with bricks was reduced.

However, when developing the numerical model, the rubber joints do not have a thickness because they are introduced as properties of the contact surfaces, so the total height to cover with bricks remains the same as in the mesoscale model with mortar joints.

In order to cover this height, the row of bricks in contact with the bottom beam will be formed by bricks with a height of 210 mm whereas the rest of the rows (12) will be formed by bricks with 212 mm of height. This means that the total *Parts* that need to be created for bricks for the mesoscale model with rubber joints are:

- Brick unit of 244x212x300 mm^3
- Half-width brick unit 122x212x300 mm^3
- Bricks in contact with the bottom beam 244x210x300 mm^3
- Brick located in the corners between bottom beam and columns 122x210x300 mm^3

The bricks whose dimensions are 122x212x300 mm^3 are located in some of the rows in contact with the columns of the reinforced concrete frame, except for the corners between the bottom beam and columns, where bricks are 122x210x300 mm^3.
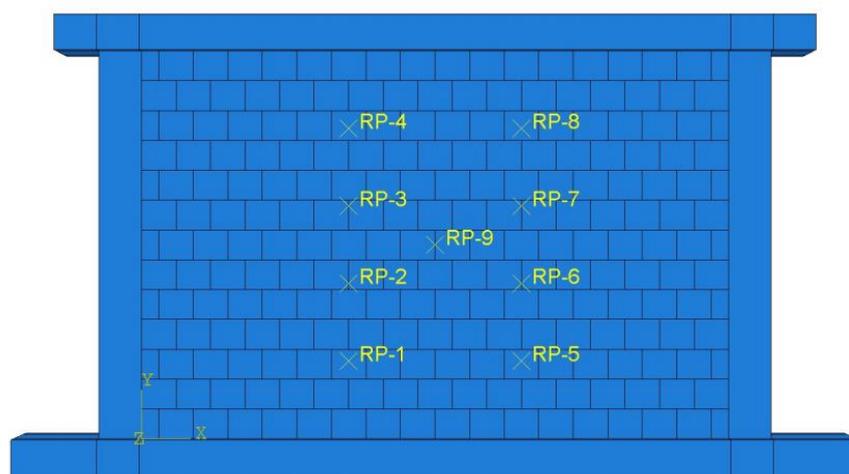

Figure 32. Mesoscale model of wall with rubber joints.

4.2.2.3. Mortar

Mortar interactions are assigned between the masonry infill and the bottom and top beams. Not only is the mortar present between beams and infill but also between the bricks of the infill, being the properties of it the ones shown in Table 11.

4.2.2.4. Rubber

Rubber interactions are introduced between bricks, creating three horizontal rubber joints, and they are also included between the columns and the masonry infill. The properties of both joints are shown in Tables 9 and 10.

5. RESULTS
5.1. Macroscale models

Macroscale models have been studied considering that the loads applied on the numerical models are: gravity, vertical load on top of the columns and the out-of-plane load introduced as a monotonic load with displacement control. This means that the results obtained will not be compared to the results of the experimental models carried out in the University of Padova, as not the same loads are being applied.

Nevertheless, macroscale models can be compared (rubber and mortar) in order to determine if there is a change in the behaviour of the wall due to the addition of deformable rubber joints. The deformed shapes obtained by Abaqus are shown in Figures 33 and 34.
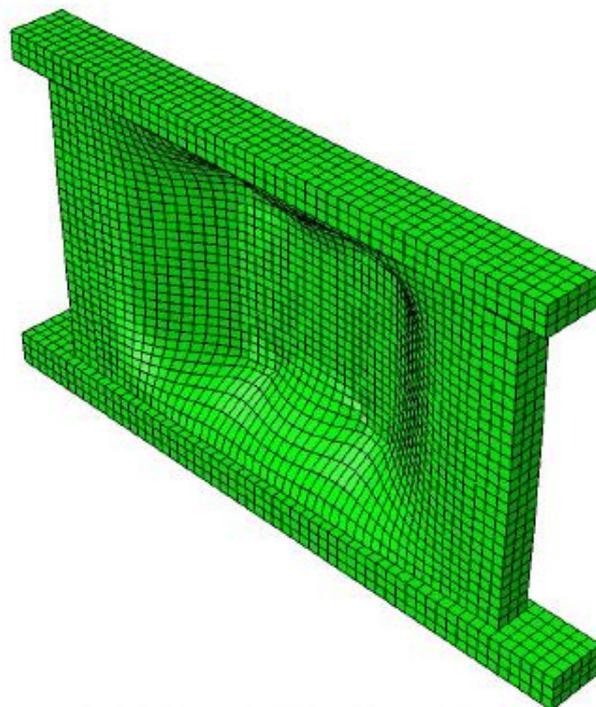

Figure 33. Deformed shape of macroscale model with mortar joints.

In Figure 33 it can be observed that the deformation of the wall is clearly caused by the application of an out-of-plane load. This macroscale model was carried out introducing one big masonry plate instead of bricks as an infill. That is the main reason why the deformed shape is showing some continuity, being the most affected area the one in the middle as that is the zone in which the out-of-plane loads were applied.
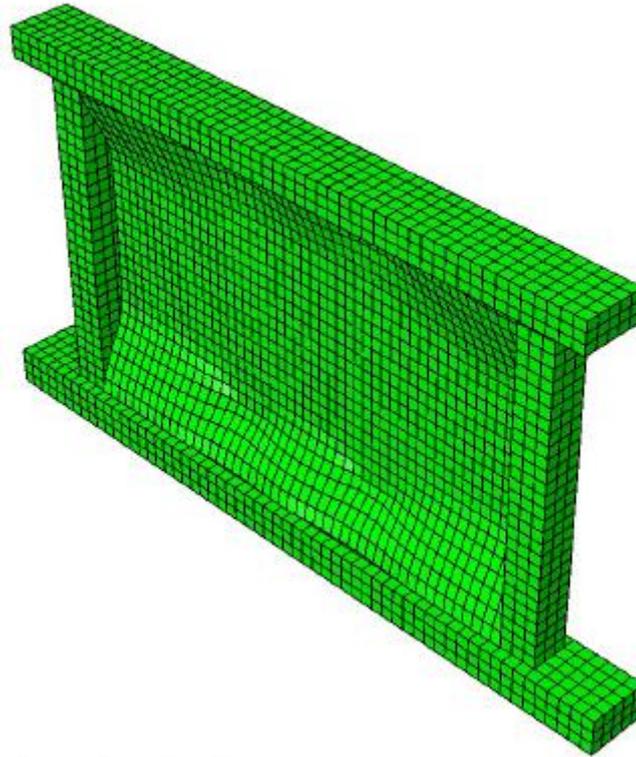
Figure 34. Deformed shape of the macroscale model with rubber joints.

The deformed shape of the model with rubber joints clearly changes compared to the model with only mortar joints. First of all, just by analysing both Figures, it seems that the deformation experienced by the model with mortar joints is higher than the deformation in the wall with rubber joints. Not only this can be said but also the clear continuity of the structure in Figure 33 is lost for the model with rubber joints. This is because the model with rubber joints was created introducing four plates of masonry instead of a big one. These four plates have masonry properties and the contact surfaces were assigned with rubber joints. The wall with rubber joints seems to be able to better accommodate the out-of-plane loads.

Apart from obtaining the deformed shapes of the structures, it has also been possible to create a graph based on the values obtained from the software Abaqus in which the out-of-plane load is represented against displacement. This graph represents both, the behaviour of the macroscale model with mortar joints and the model with rubber joints, and it appears in Figure 35.
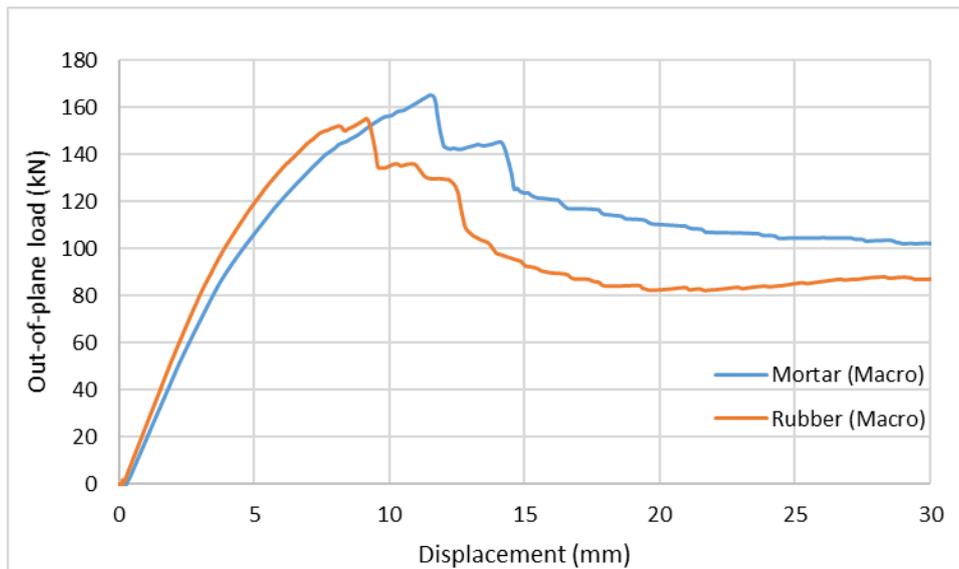
Figure 35. Out-of-plane load-displacement graphs for macroscale models.

From Figure 35 it can be said that, despite not having the same values, both graphs kind of follow the same pattern. The model with mortar joints reached a maximum strength of 165.47kN with an inflection in the out-of-plane direction of 11.49 mm. However, the maximum strength reached for the model with rubber joints is 155.37 kN with a deflection of 9.18 mm in the out-of-plane direction. This lower value of strength reached by the wall with deformable joints can be due to a reduced compressive stiffness of the enclosure with rubber joints.

Nevertheless, according to the results shown in Figure 35, it seems that the wall with rubber joints is showing a higher initial stiffness than the wall with mortar joints. This behaviour is not representing the actual performance of deformable joints, as with only out-of-plane loads acting on the wall, the stiffness should be lower for the wall with rubber joints compared to the one with mortar joints. What is more, the deflection associated to the maximum strength should be higher for the wall with rubber joints than for the wall with mortar joints because of the reduced compressive stiffness of the wall with deformable joints.

In the results of the experimental models collected in Figure 20, it is shown that the walls that include deformable joints presented a higher initial stiffness than the wall with regular mortar joints. However, this experiment was carried out considering first an in-plane load applied on the wall and then an out-of-plane load which was introduced in the model once it had been damaged by the in-plane load. According to Verlato et al., (2016) in the case of having both in-plane and out-of-plane loads, the behaviour of the walls is reversed, showing a higher initial stiffness the walls with deformable joints. However, for the case of having only out-of-plane loads, the initial stiffness of the wall should be higher for the mortar case studied, which means that the results obtained in Figure 35 are not representing the actual behaviour of the walls against out-of-plane loads.

Some limitations of the numerical macroscale models may be due to a non-accurate introduction of the interface rubber and mortar properties or even because of modelling the masonry with big plates instead of bricks.

5.2. Mesoscale models

Mesoscale models were carried out considering both in-plane and out-of-plane loads. This means that the results obtained can be compared with the ones related to the experimental models.
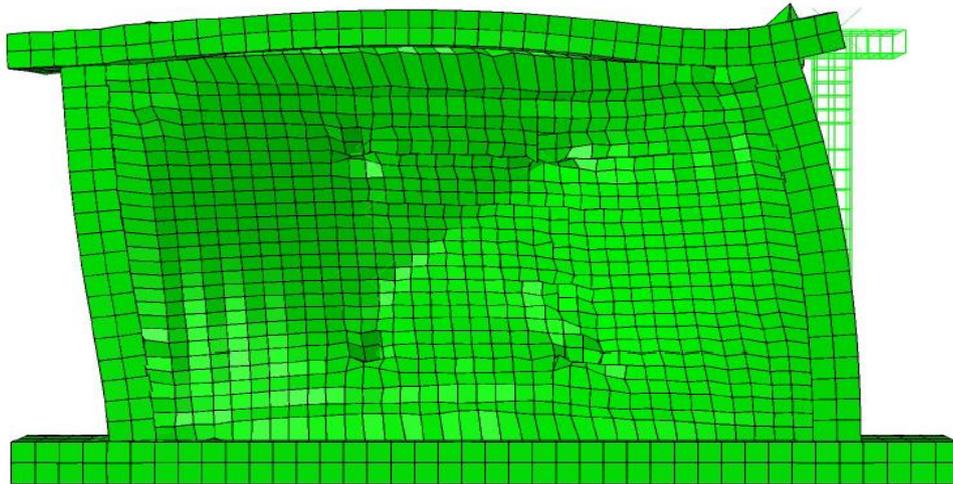
Figure 36. Deformed shape of the mesoscale model with mortar joints.

In Figure 36 it can be observed how the deformed shape of the structure is due to both in-plane and out-of-plane loads. These loads represent a seismic event and, in the centre of the structure, a cross can be observed which is the main pattern that the cracks follow in a structure after being damaged by the action of an earthquake. However, one of the diagonals of the cross is more evident than the other one. This is because in the numerical model, the out-of-plane load was applied after the in-plane load, but the in-plane load was still acting when the out-of-plane was introduced. In the experimental models, once the infill had been damaged by the in-plane load, this load was brought back to zero and the out-of-plane load was then applied. This is a difference between the numerical mesoscale models and the experimental ones.
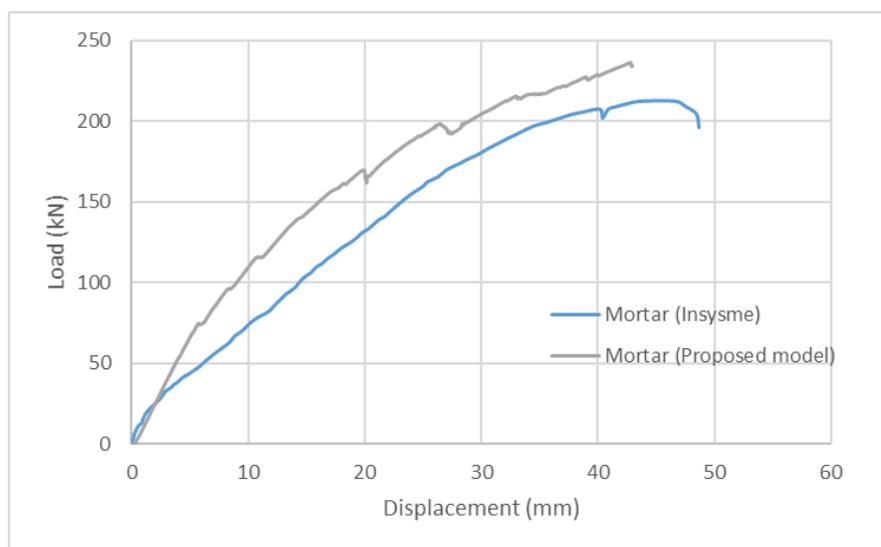
Figure 37. Load-displacement results for mortar models.

Figure 37 shows the comparison between the behaviour of the mortar mesoscale model and the experimental model with mortar joints. Both graphs follow the same pattern but for the numerical model the ultimate strength does not seem to have been reached.

The maximum strength that the numerical model reached is 236.25 kN whereas the maximum strength reached in the experimental model is 212.51 kN. The numerical model seems to have a higher stiffness compared to the experimental one, so apparently the experimental mortar model was more flexible. This main difference can be due to the fact of introducing the surface interaction properties in the software without total accuracy. Replicating a real model in a software is not simple and, after obtaining the results, some of the parameters introduced in the model need to be changed so that both curves get as closer as possible. This means that it is a long process that implies modifying the parameters of the interaction properties until finally obtaining a good result. At that point, the numerical model would be representing the behaviour of the experimental model.

Not only can this difference be due to the materials or interaction properties introduced in the model but also because of the mentioned fact that in the numerical model the out-of-plane load started acting after the in-plan load, but this last load was not reduced to zero. Both in-plane and out-of-plane loads acted together for the numerical model.

For those reasons, it would be interesting to create again the model, changing some of the interfaces' parameters and reducing the in-plane load to zero before the out-of-plane load starts acting. This is how more accurate results will be achieved.
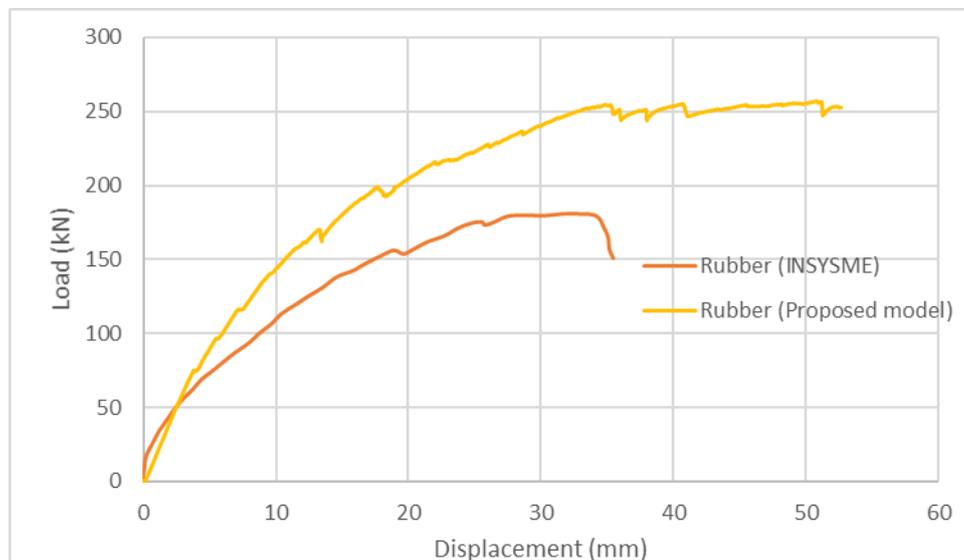

Figure 38. Load-displacement results for rubber models.

Figure 38 shows the results obtained for the rubber mesoscale model and the experimental model with deformable joints. The same issues happen as in the mortar models. The numerical model seems to have a higher initial stiffness and, although the pattern both graphs follow is similar, it is not exactly the same.

In this case, the maximum strength reached by the numerical model is 260.59 kN. Again, the differences between the graphs may be due to the properties of the rubber interaction surfaces introduced in the numerical model as well as to the in-plane and out-of-plane loads acting together instead of applying one after the other has been reduced to zero.

Developing a new numerical model changing some parameters as well as the loads might be a good solution in order to obtain a more accurate model.
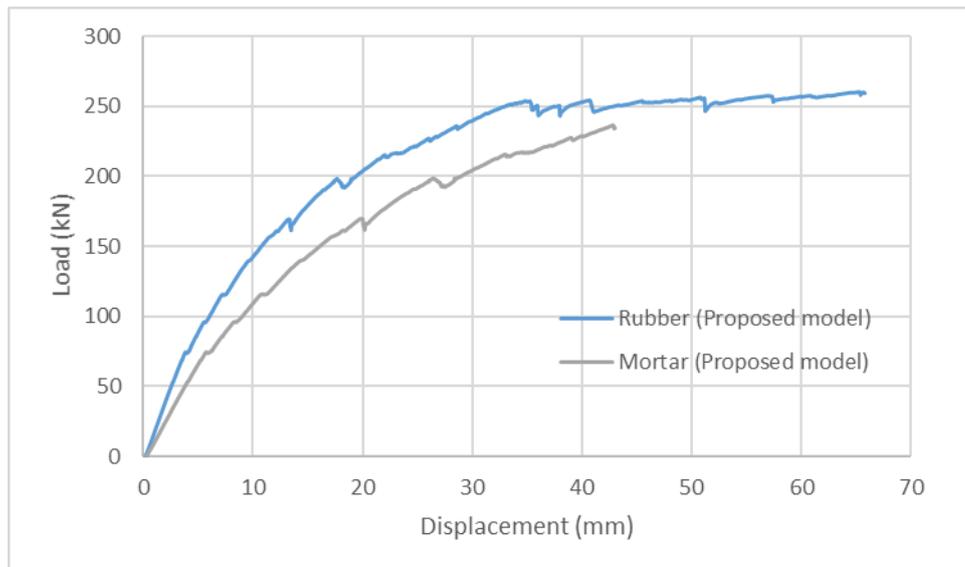

Figure 39. Load-displacement results for mesoscale models.

Figure 39 collects the load-displacement results for both mesoscale models; with mortar and with deformable rubber joints. It can be observed that the model with deformable joints shows a higher initial stiffness compared to the model with mortar joints. Comparing these results to the results collected in Figure 20 for the experimental models, it does make sense that the rubber model shows a higher initial stiffness, as that is what happened in the experimental tests carried out in the University of Padova.

It must be said that, although similar results were obtained for the macroscale models (Figure 35) where the rubber model showed a higher stiffness, now the results do make sense because there are two loads acting; in-plane plus out-of-plane, and, as it had been mentioned before, in the experimental case where in-plane and out-of-plane loads were considered, the rubber model showed a higher initial stiffness.

This means that, despite not being the most accurate representation of the experimental models, comparing the two mesoscale models is a valid option as they show similar results to the experimental models.

In general, it can be said that the numerical models developed for this project need checking and some modifications in order to obtain better results. It is important to mention that the deformable rubber joints do imply an improvement for walls with in-plane loads. In walls where only out-of-plane loads are acting, the addition of rubber joints is not the best option in order to improve their behaviour. However, as seismic actions include both in-plane plus out-of-

plane loads, including rubber joints in masonry structures is a good option in order to reduce the damage that they may suffer.

It can also be interesting studying the location of the rubber joints. In this project, rubber joints were introduced as horizontal and vertical layer, but maybe there are other dispositions in which the structure might improve its behaviour and so they would be interesting to study.

6. APPLICATION TO SPAIN

6.1. Area of study

Once the numerical models were created and the results were obtained, it is possible to study an application case of a masonry infill wall in the province of Alicante in Spain.

Alicante is a Spanish province located in the south-east of the country and some of the municipalities of this province are located in areas of high seismic hazard according to the Ministerio de Fomento (2009).

Figure 40. Map of Spanish seismic hazard zones (Ministerio de Fomento, 2009).

In Figure 40, the location of Alicante is shown with a red square. As it can be observed, it is located in a dark grey area which means that it is a high seismic hazard zone, with a high value of basic seismic acceleration (a_b).

6.2. Seismic acceleration

According to the Ministerio de Fomento (2009), the basic seismic acceleration is a characteristic value of the horizontal acceleration of the surface of the ground. It is expressed in relation to the value of gravity (g) and for the south of Alicante its value is:

$$a_b \geq 0.16g$$

The map of Spanish seismic hazard zones not only provides the distribution of values of the basic seismic acceleration but also the contribution coefficient (K), which takes into account the influence of the different types of earthquakes expected in the seismic hazard of each location.

Orihuela is a city located in the province of Alicante with a high ratio between the basic seismic acceleration and the gravity. According to the Ministerio de Fomento (2009), its characteristics are:

$$\frac{a_b}{g} = 0.16$$

$$K = 1$$

This city has been selected in order to create a masonry infill wall that will have to withstand seismic loads equivalent to the ones that may occur in Orihuela.

However, the force acting on the wall is not provided by the basic seismic acceleration but by what is called calculus' seismic acceleration (a_c). According to the Ministerio de Fomento (2009), the value of this acceleration can be obtained by the following equation:

$$a_c = S * \rho * a_b$$

Where:

S is a coefficient of amplification of the ground. Its value depends on a_b and ρ.

ρ is a dimensionless coefficient of risk, and its value is 1.0 for constructions of normal importance.

a_b is the basic seismic acceleration

The coefficient of amplification S adopts the following value for $0.1g < \rho * a_b < 0.4g$:

$$S = \frac{C}{1.25} + 3.33 * \left(\rho * \frac{a_b}{g} - 0.1\right) * \left(1 - \frac{C}{1.25}\right)$$

Where:

C is the ground coefficient and it depends on the geotechnical characteristics of the soil. The Ministerio de Fomento (2009) classifies soils into four types:

- Type I: Compact rock, very dense granular soil. (C = 1)
- Type II: Very fractured rock, dense granular soils or hard cohesive soils. (C = 1.3)

- Type III: Granular soils of medium compressibility or cohesive soils with firm consistency. (C = 1.6)
- Type IV: Loose granular soil or soft cohesive soil. (C = 2)

As the geotechnical characteristics of the soil are unknown and, in order to be more conservative, the adopted value of C is 2, which is the value for Type IV soils.

Once this value is known, it is possible to obtain the coefficient of amplification S:

$$S = \frac{C}{1.25} + 3.33 * \left(\rho * \frac{a_b}{g} - 0.1\right) * \left(1 - \frac{C}{1.25}\right)$$

$$S = \frac{2}{1.25} + 3.33 * (1 * 0.16 - 0.1) * \left(1 - \frac{2}{1.25}\right) = 1.48$$

And so, the calculus' seismic acceleration is:

$$a_c = S * \rho * a_b$$

$$a_c = 1.48 * 1 * 0.16 * 9.81 = 2.32 \, m/s^2$$

The spectrum of elastic response is defined by the following equations (Ministerio deFomento, 2009):

If $T < T_A$ $\qquad\qquad\qquad$ $\alpha(T) = 1 + 1.5 * \frac{T}{T_A}$

If $T_A \leq T \leq T_B$ $\qquad\qquad$ $\alpha(T) = 2.5$

If $T > T_B$ $\qquad\qquad\qquad$ $\alpha(T) = K * \frac{C}{T}$

Where:

$\alpha(T)$ is the value of the normalised spectrum of elastic response

T is the period of the oscillator in seconds

K is the coefficient of contribution previously calculated

C is the ground coefficient, obtained considering the geotechnical characteristics of the soil

$T_A \, and \, T_B$ are the characteristic periods of the spectrum, whose values are:

$$T_A = K * C/10$$

$$T_A = 1 * 2/10 = 0.2 \, s$$

$$T_B = K * C/2.5$$

$$T_B = 1 * 2/2.5 = 0.8 \, s$$

The spectrum for the studied area is shown in the following Figure:
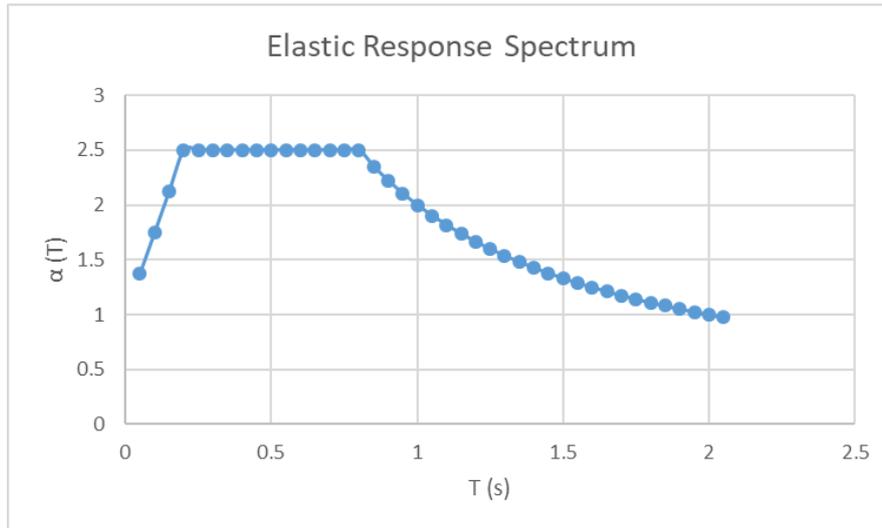
Figure 41. Elastic Response Spectrum for the area of Orihuela in Spain.

In order to be more conservative, the period adopted lies between T_A and T_B so that the value of α is the maximum, which is 2.5.

The acceleration is then:

$$a = a_c * \alpha = 2.32 * 2.5 = 5.8 \; m/s^2$$

6.3. Acceleration obtained from numerical models

Once the maximum values of the forces are known for the numerical models, it is possible to obtain the acceleration that the force induces in the structure following Newton's second law:

$$F = m * a$$

This is a simplification process. It is actually not as simple as applying Newton's second law but by doing it, it is possible to compare both, the acceleration obtained from the analytical models and the seismic acceleration of the studied area.

In order to obtain this acceleration, the mass of the structure must be known. The mass of the wall is calculated knowing the volumes and densities of the masonry, concrete and steel elements of the wall. The volumes of each material have been calculated considering the dimensions of the structure shown in Figure 22, and they are collected in Table 12.

Volumes	
Concrete	2.056 m^3
Steel	0.053 m^3
Masonry	3.427 m^3

Table 12. Volumes of the materials included in the numerical model.

In order to simplify these calculations, the density of mortar and rubber have not been considered, assuming the masonry infill forms a big panel. This is a conservative assumption as the density of the masonry is greater than the densities of mortar and rubber.

The densities of each material are the same as the ones introduced in the software Abaqus, and the values are:

Densities	
Concrete	2500 kg/m^3
Steel	7800 kg/m^3
Masonry	2100 kg/m^3

Table 13. Densities of the materials included in the numerical model.

The mass of the structure can now be obtained after knowing the densities and volumes of the different materials:

$$Mass = \rho_c * v_c + \rho_s * v_s + \rho_m * v_m$$

$$Mass = 2500 * 2.056 + 7800 * 0.053 + 2100 * 3.427 = 12750.1 \ kg$$

The value of the force is obtained from the results of the mesoscale models. In order to be more conservative, the maximum load is assumed as 260.59 kN, which is the maximum strength obtained in the mesoscale model with rubber joints (Figure 38).

Once the mass of the structure and the value of the force are known, the acceleration can be obtained:

$$a = F/m$$

$$a = \frac{260590}{12750.1} = 20.44 \, m/s^2$$

The value of the acceleration obtained from the numerical models is approximately 3.5 times bigger than the value of acceleration calculated following the Spanish code.

This means that if the numerical model of the wall was able to withstand the acceleration without collapsing, then a similar wall located in the city of Orihuela in Spain will be able to resist without collapsing during a seismic event.

However, this is only an approximate calculation for different reasons. First of wall, the density of the rubber joints has not been taken into account in order to obtain the mass of the wall. Apart from that, a real structure is a non-linearity problem where the boundary conditions differ from the ones considered in the numerical models. These models are just a simplification, so the structure should be studied under a different approach before confirming that it is totally safe from collapsing during a seismic event.

7. REFERENCES

INSYSME (2013) *Innovative Systems for Earthquake Resistant Masonry Enclosures in RC Buildings. Influence of the global response of the structure on the local response of the non-structural element.* Università di Padova.

INSYSME. (n.d.) *INSYSME Project.* Available from: http://www.insysme.eu/ [Accessed 24th April 2019].

Pujol, S., Benavent-Climent, A., Rodríguez, M. & Smith-Pardo, J.P. (2008) *Masonry infill walls: an effective alternative for seismic strengthening of low-rise reinforced concrete building structures.* The 14th World Conference on Earthquake Engineering, 12-17 October 2008, Beijing, China.

Verlato, N., Guidi, G., da Porto, F. & Modena, C. (2016) Brick and Block Masonry – Trends, Innovations and Challenges. *Innovative systems for masonry infill walls based on the use of deformable joints: Combined in-plane/ out-of-plane tests.* 1359 – 1366.

British Standards Institution (2016) BS EN 998-2:2016. *Specification for mortar for masonry. Part 2: Masonry mortar.* London, BSI.

Norme Techniche per le Costruzioni (2008) *Decreto Ministeriale 14 Gennaio 2008.* Available from: http://www.ingegneriasoft.com/NTC2008_Norme_tecniche_per_le_costruzioni.htm [Accessed 24th April 2019].

Calabria, A., Guidi, G., da Porto, F. & Modena, C. (2016) Brick and Block Masonry – Trends, Innovations and Challenges. *Innovative systems for masonry infill walls based on the use of rubber joints: Finite element modelling and comparison with in-plane tests.* 1155 – 1161.

LATERIZIO. (n.d.) *Sistemi costruttivi innovativi per tamponature in laterizio basati sull'utilizzo di giunti deformabili.* Available from: http://www.laterizio.it/cil/ricerca/362-sistemi-costruttivi-innovativi-per-tamponature-in-laterizio-basati-sull-utilizzo-di-giunti-deformabili.html [Accessed 25th April 2019].

P. Camacho, P., & R. Hallett, S. (eds.) (2015) *Numerical Modelling of Failure in Advanced Composite Materials.* Cambridge, Elsevier: Woodhead Publishing.

Ministerio de Fomento (2009) *Norma de Construcción Sismorresistente: Parte general y edificación (NCSE-02).* Madrid, Centro de Publicaciones. Secretaría General Técnica.